ELSEVIER

Chemical Geology 203 (2004) 1–27

CHEMICAL GEOLOGY
INCLUDING
ISOTOPE GEOSCIENCE

www.elsevier.com/locate/chemgeo

Geochemistry of red residua underlying dolomites in karst terrains of Yunnan-Guizhou Plateau I. The formation of the Pingba profile

Hongbing Ji[a,b,c,*], Shijie Wang[a], Ziyuan Ouyang[a], Shen Zhang[c], Chenxing Sun[a], Xiuming Liu[a], Dequan Zhou[a]

[a] *The State Key Laboratory of Environmental Geochemistry, Institute of Geochemistry, Chinese Academy of Sciences, Guiyang 550002, China*
[b] *Resource, Environment and GIS Key Laboratory of Beijing City, Department of Geography, Capital Normal University, Beijing 100037, China*
[c] *Key Laboratory of Environmental Biogeochemistry, Institute of Geographic Sciences and Natural Resources Research, Chinese Academy of Sciences, Beijing 100101, China*

Received 18 December 2001; received in revised form 27 August 2003; accepted 28 August 2003

Abstract

We present a set of bulk chemical and mineralogical compositions of the Pingba red residua on karst terrains of the Yunnan-Guizhou Plateau that show evidence pertaining to the source and to evolution of the profile. The known potential sources of clay-rich deposits on the plateau include: (1) Triassic dolomites, (2) Quaternary sediments, (3) Chinese loess, (4) Early Pliocene–Late Holocene volcanic ash (although the existence of volcanic ash is not supported by geological or mineralogical data), or a mixture of the four sources. The mineralogical compositions of the profile have shown an obvious inheritance relationship between the regolith and insoluble residues from the underlying dolomites, without allochthonous components involved. In the regolith, the contents of Al_2O_3 and Zr are fairly constant and both the TiO_2/Al_2O_3 and Fe_2O_{3T}/Al_2O_3 ratios are consistent with those of bedrock below in the profile. The chemical index of alteration (CIA) for the profile varies from 84 to 94. An obvious variation is only found in the lower regolith. In the Al_2O_3-CaO* + Na_2O-K_2O (A-CN-K) triangular diagram, almost all the samples are concentrated, and cannot be distinctly distinguished, close to the A-K joint, and they tend to the A end. The SiO_2/Al_2O_3 ratio in the samples from the regolith is less variable and low (≈ 1), but the K_2O/Na_2O ratio is very variable (2–18). The above two ratios are quite different from those of PAAS, upper continental crust (UCC) and Chinese loess. Average UCC-normalized spiderdiagrams for the samples from the regolith and the insoluble residues in the dolomites share much in common with respect to element distribution pattern. The ratios of mobile to immobile elements (Ca/Al, Mg/Al, Na/Al, K/Al and Mn/Al) and between the immobile elements (Al/Zr, Ti/Zr and Ti/Nb) reflect the characteristics of in situ weathering rather than a sedimentary origin. The above lends great support to a cognate relation between the dolomite and its overlying regolith.

The chemical weathering of dolomite can be divided into two stages in the major element and high field strength element (HFSE) diagrams—namely for "leaching-accumulating trend" and "weathering trend". The research results of

* Corresponding author. Resource, Environment and GIS Key Laboratory of Beijing City, Department of Geography, Capital Normal University, Beijing 100037, China. Tel.: +86-10-6890-7073.
E-mail address: hbji@sina.com (H. Ji).

0009-2541/$ - see front matter
doi:10.1016/j.chemgeo.2003.08.012

this paper demonstrate that the Pingba red residua is a typical in situ chemical weathering crust and material sources of the profile are derived from underlying Triassic dolomites. The previously postulated two-stage development model for red residua in the karst terrain can be discriminated clearly, among them, the change of chemical composition occurs notably in the transition periods of the two stages. Moreover, it is the leaching processes that have an important meaning in the formation of horizons of the soil and ferruginous crust from the profile.

Keywords: Elements; Weathering; Material sources; Red residua; Karst terrain

1. Introduction

Rock weathering, soil formation and sediment deposition are the most important supergenic geological processes. Although chemical weathering is a continuous process, its evolution leads to soil forming. The sand- and mud-grade materials produced in profile by in situ chemical weathering are a major source of sediments in a region. The content and nature of the parent rock in sediments have been determined by geochemical information included in the degree of weathering to which primary mineral in profile was subjected. At present, a wealth of data is available about chemical weathering of nonsoluble rocks (e.g., magmatic and metamorphic rocks) and terrestrial deposits (e.g., loess) (Middelburg et al., 1988; Banfield and Eggleton, 1989; Braun et al., 1990, 1998; Macfarlane et al., 1994; Nesbitt and Markovics, 1997; Gallet et al., 1998; White et al., 1998; Panahi et al., 2000; Sharma and Rajamani, 2000a; Aubert et al., 2001; Jahn et al., 2001). But the chemical weathering of soluble rock (carbonate rock for example) in karst areas is less understood.

Chemical weathering of rocks is one of the major processes that modify the earth's surface and is one of the critical processes in the geochemical cycling of elements (Berg, 1932). The fractionation, mobilization and redistribution of trace elements during weathering are particularly complicated, because they are affected by various processes such as dissolution of primary minerals, formation of secondary phases, redox processes, transport of material, coprecipitation and ion exchange among various minerals (e.g., Middelburg et al., 1988 and references therein). The behavior of elements in rock weathering processes, and element distributions in weathering profile are not very well understood (Sharma and Rajamani, 2000b). Because many physical and chemical conditions in weathering processes are peculiar for a region and the geochemical behavior of many elements is very hard to summarize, especially in the soil environment, it is difficult to constrain the sources of soil components due to variable solubility and mobility of cations (Borg and Banner, 1996). Many geochemical studies of soils have focused on chemical elements from a single volcanic and metamorphic weathering regolith source (e.g., Nesbitt, 1979; Middelburg et al., 1988; Marsh, 1991); however, in many geological setting multiple sources contribute to soil via fluvial and eolian transport mechanisms (e.g., Brimhall, 1988; Maynard, 1992). Unfortunately, the geochemical compositions of these sources contributing to soil chemistry are difficult to determine.

Most carbonates have little association with clastic material or biogenic opal (Blatt et al., 1980) because the turbidity associated with clastic sedimentation suppresses the biogenic activity required for carbonate deposition. An upper limit of clastics in typical carbonates is about 5%. The siliceous components (or non-carbonate components—namely insoluble residues) in the carbonates are released as the carbonates dissolve. If the terrain is flat, siliceous soils develop over the carbonates, while on slopes, physical erosion limits soils to a thin veneer (e.g., weathering skin, desert varnish) (Legros, 1992; Stallard, 1995). The weathering of the carbonate rock we used in this paper is the same as the karst-related weathering called by Tardy (1997). Generally, the weathering of calcite (or dolomite) is summarized in a congruent dissolution type (e.g., Drever, 1997), but the weathering of carbonate rocks under the natural background is not full understood. Aluminosilicate

weathering differs from weathering of carbonate rock in several important aspects: firstly, the dissolution of carbonate rocks is not appreciably affected by the topography, e.g., the dissolution of carbonates under high relief (or elevation) and low relief conditions occurs with the formation of karst features (Berner, 1995). Secondly, the dissolution rate of carbonates is greater than that of aluminosilicates, e.g., 10^6 orders of magnitude greater than that of granite in the laboratory experiments under neutral pH condition (Plummer et al., 1979; Lasage, 1984; Drever and Clow, 1995). Thirdly, the weathering of carbonate rocks relies more on the volume of runoff, e.g., the faster dissolution of carbonates under higher runoff conditions (Berner, 1995). Fourthly, the processes of carbonate rock weathering are comparatively complicated, e.g., we divided the weathering process of carbonate rocks into two stages: one for the leaching of carbonate rocks and accumulation of insoluble residues (forming residue soils) and the other for the weathering of the residue soils (Wang et al., 1999; Ji et al., 2000). Fifthly, the genesis of clay-rich soils underlying carbonate rock has been debated for several years (Muhs et al., 1987 and references therein). At present, five hypotheses have been suggested interpreting the formation of the clay-rich soils: (1) the accumulation of insoluble residues from the underlying carbonate rocks (Ahmad et al., 1966; Clarke, 1966; Ahmad and Jones, 1969; Isphording, 1978); (2) soils formed by processes of dissolution, replacement, precipitation and infilling etc., of underlying carbonate rocks (Monroe, 1986); (3) the deposition on lower carbonate rock surfaces of fluvially transported clays (or diluvium, talus and alluvium accumulation) from topographically higher positions (Zans, 1959; Chubb, 1963); (4) the weathering of volcanic ash which has fallen on the carbonate rock surfaces (Comer, 1974); (5) the weathering of fine-grained eolian sediments originating in distant regions (Prospero, 1981; Muhs et al., 1987; Muhs et al., 1990; Borg and Banner, 1996).

Laterites, including terrigenous red soils (e.g., bauxites, ferricretes and nodular soils, etc.) are estimated to cover over one-third of all the emerged lands of the world (Nahon, 1986), and result from long-term exposure of cratonic rocks to intense weathering conditions in the tropical and subtropical climatic districts. In southern China, they also spread widely up to 2,200,000 km^2, and record rich information about the history of regional ecological and environmental change (Zhao and Shi, 1983). Although many research results have been obtained about the Chinese laterites since 1930s (e.g., Teilhard de Chardin et al., 1935; Young et al., 1938; Ceng, 1958; Xi, 1965; Yen, 1983; Zhu, 1993; Huang, 1996; Sui and Yao, 2000), red residua in karst terrains of southern China, which are extensively developed on plantation surfaces with different elevations since the Cenozoic Era (Huang, 1996; Li et al., 2000, 2002), are yet poorly understood, especially about its material sources and evolution.

The purpose of this paper is to investigate the weathering mechanism of dolomites in karst terrains, under warm-humid subtropical climate condition in upland of karst terrains, Guizhou Province. Emphasis is given particularly to the material sources for the red residua, geochemical processes for the formation of the soil profile. Moreover, we set an example for further inquiring material sources of clay-rich residua widespread in carbonate rock areas of southern China in this paper.

2. Description of the study area

2.1. Geological and geographic setting

The study area is on Yunnan-Guizhou Plateau (Fig. 1). Guizhou Province is part of the Yangtze Platform. It contains mainly Proterozoic clastic sedimentary rocks and Palaeozoic to Upper–Middle Triassic marine carbonate rocks; Post Triassic rocks are mainly fluvial (Guizhou Provincial Geological Survey Team, 1995). Uplift took place since the middle–late Triassic. The Cenozoic was dominated by the equatorial and East Asia summer monsoons and Siberia–Mongolia winter monsoon. These monsoons strongly influenced the soil distribution, with red soil occurring in the west and yellow soil occurring in the wet and moist east.

The vast moist karst terrain in southwestern China covers central Guizhou Province, eastern Yunnan, southern Sichuan and the western

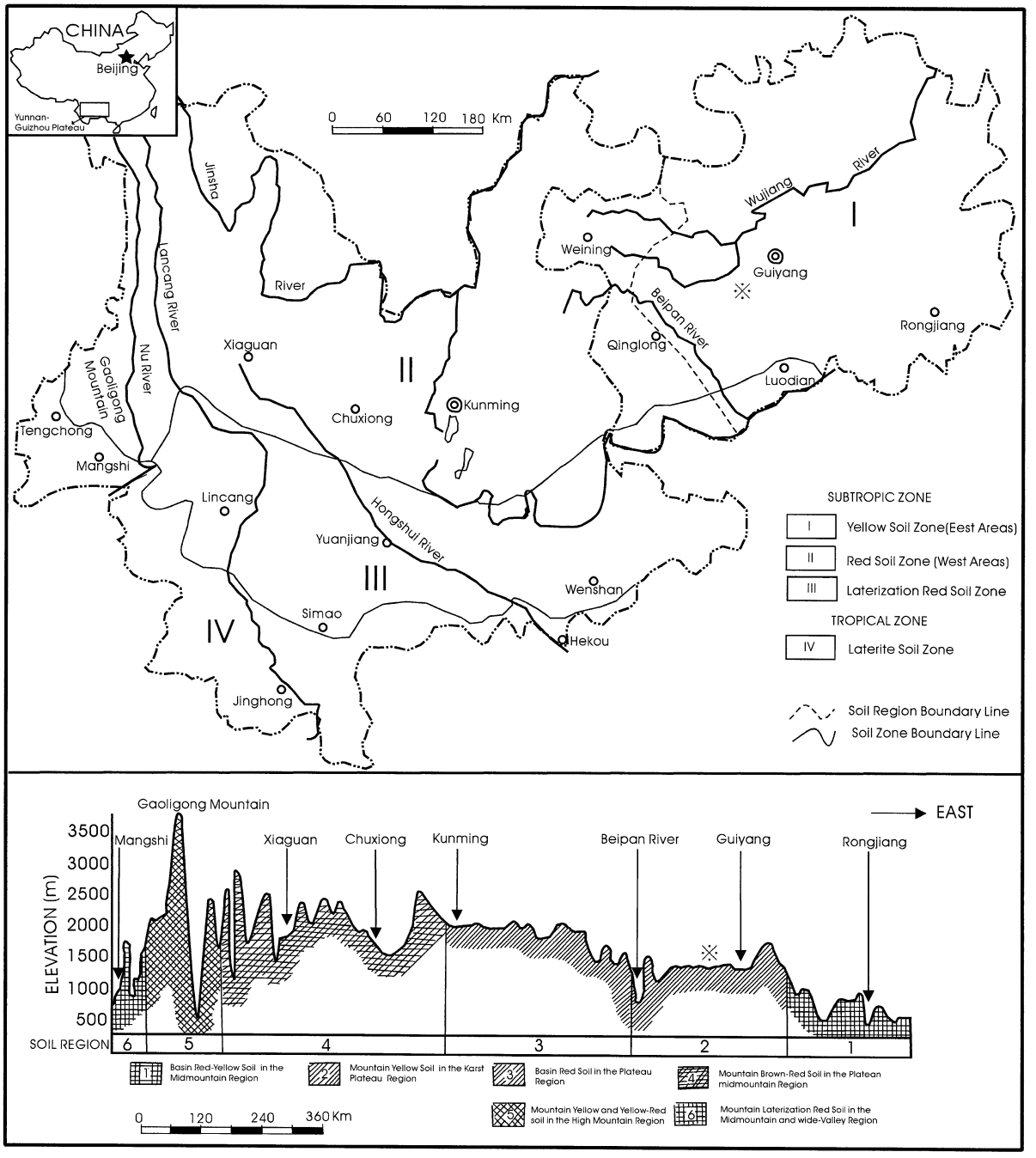

Fig. 1. The map of soil distribution in horizontal and vertical profiles for the Yunnan-Guizhou Plateau modified from Zou (1965). Stat indicates the location where the Pingba profile has been sampled.

Guangxi, Hunan and Hubei provinces. At 500,000 km^2, this is one of the largest continuous distributions of karst in the world (Yuan, 1992). Here, red residua with the development of yellow soils, red soils and laterites, are extensive and form one of largest continuously developed ancient weathering crusts on the earth's surface (Xi, 1990; Zhu, 1993).

2.2. Analysis of potential soil sources

Little is known about the genesis of clay-rich soils on the karst terrains of Guizhou Province. In their study above the red residua in southern China, Xi (1965, 1990, 1991) considered that the uniformly massive red clays developed in the various areas of Guizhou Province are the products of weathering of Quaternary

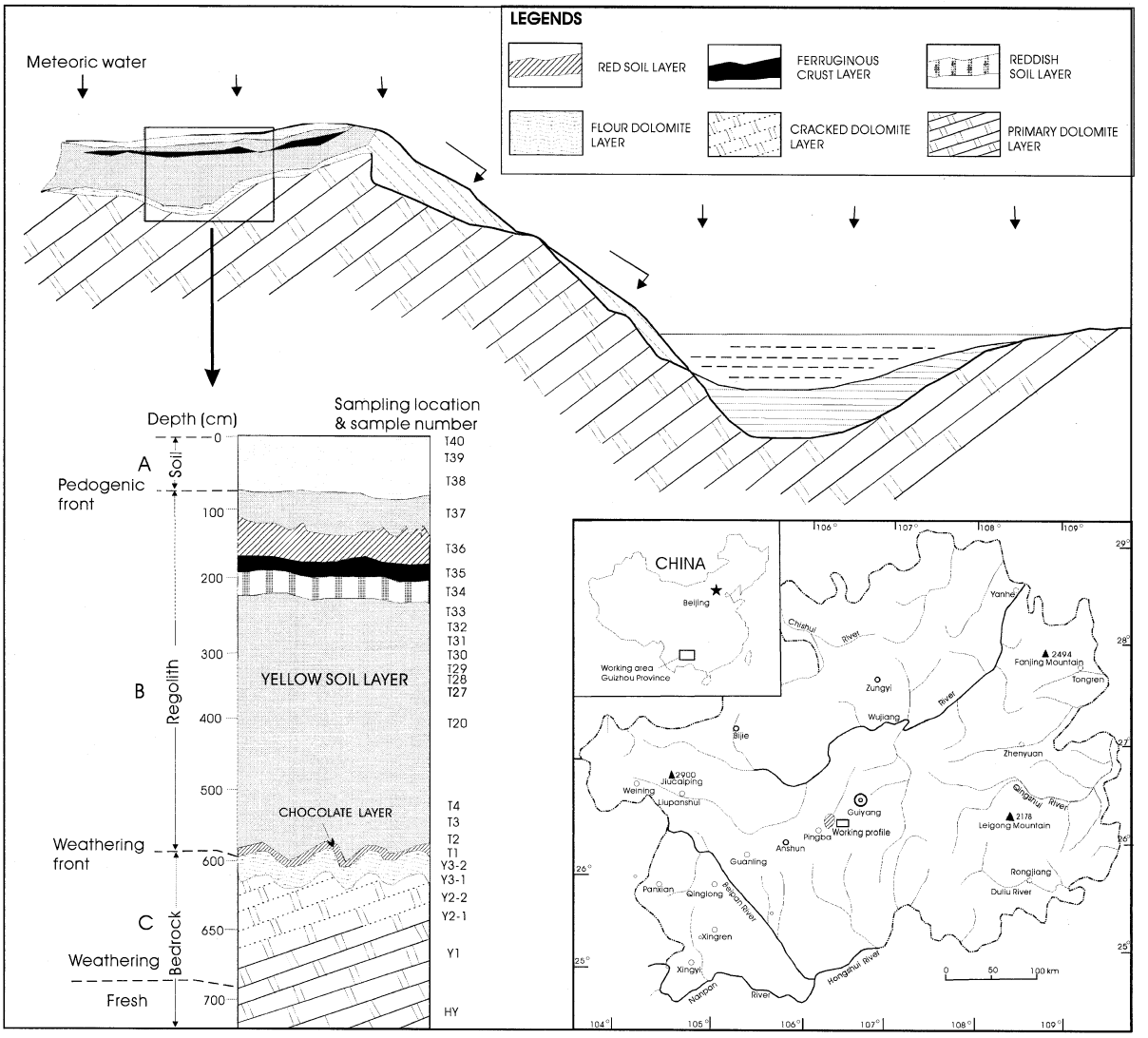

Fig. 2. The simplified sketch of the Pingba profile showing the location of the sampling and sample numbers, those not listing the number samples are a space of 10 cm between each two adjacent sampling. (Below right) the map of the Guizhou showing location of the profile (after Lin et al., 1994) and referred to in the text.

deposits. Liu et al. (1985) thought that the loess of China could extend to the vast areas including the south of the Yangtze River (south to 30°N), but whether it would exert some influences on this region is still an open question. According to historic records, "the soil rain" (including dust storm and eolian dust, which represent loess and soil developed from loess source) was reported in Guangdong, Guangxi and Fujian and such soil rain could extend to the vicinity of the North Cancer (Zhang, 1982). Therefore, it was believed that

Table 1
Major and trace element contents of bulk samples from the Pingba dolomite profile

Samples[a]	HY	Y1	Y2-1	Y2-2	Y3-1	Y3-2	YT1	YT2	YT3	T1	T2	T3
SiO_2	0.98	1.46		1.04		0.85	51.71	51.64	45.86	34.79	36.90	33.25
TiO_2	0.06	0.02		0.02		0.06	1.01	1.11	0.90	0.87	0.76	0.77
Al_2O_3	0.09	0.05		0.47		2.38	22.18	20.99	25.03	27.53	29.67	33.40
Fe_2O_3	0.11	0.10		0.06		0.76	5.76	6.17	11.18	8.85	8.60	10.94
FeO	0.02	0.05		0.05		0.10	0.44	0.43	0.52	0.55	0.60	1.06
MnO	0.005	0.004		0.004		0.03	0.01	0.01	0.02	0.57	0.29	0.40
MgO	20.00	19.90		20.50		19.00	2.20	2.10	1.50	1.70	1.30	1.10
CaO	31.60	30.60		35.20		35.60	0.60	0.80	0.20	1.40	0.60	0.40
Na_2O	0.05	0.06		0.04		0.06	0.45	0.32	0.33	0.18	0.83	0.49
K_2O	0.05	0.02		0.03		0.16	5.90	5.80	4.66	3.26	2.12	1.95
P_2O_5	0.03	0.03		0.03		0.04	0.04	0.05	0.15	0.47	0.15	0.25
CO_2	45.50	40.17		40.36		38.70						
LOI	0.75	6.70		1.40		1.70	8.92	9.65	9.00	18.88	17.34	15.35
Total	99.24	99.16		99.20		99.44	99.22	99.07	99.35	99.05	99.16	99.36
CIA[b]							72	73	82	84	87	92
Sc	1.16	1.19	1.17	1.94	1.30	1.30	21.41	19.15	12.75	38.17	49.96	82.55
V	3.07	3.25	2.86	1.71	3.97	4.34	167.37	156.90	134.65	198.78	254.53	284.02
Cr	20.78	22.55	1.45	1.70	1.19	22.58	372.23	254.40	106.24	74.23	125.27	131.97
Co	1.34	1.30	0.87	1.24	1.08	1.53	13.59	16.40	18.89	53.72	64.72	199.35
Ni	16.03	17.06	4.98	4.75	3.89	15.53	76.69	98.97	129.20	153.21	213.08	252.02
Cu	7.46	8.95	6.13	2.92	6.52	9.50	103.24	152.69	137.79	232.38	143.88	173.50
Zn	19.58	11.27	9.54	2.30	5.46	7.93	201.75	201.35	167.79	− 414.62	412.63	471.63
Ga	0.19	0.18	0.14	0.18	0.50	0.83	39.73	36.41	27.94	63.32	52.3	50.06
Rb	1.10	1.12	0.83	0.81	1.67	2.01	230.28	210.03	151.98	155.72	137.37	116.90
Sr	65.92	70.00	65.47	62.53	72.36	57.84	89.76	77.49	68.65	62.26	61.12	64.55
Y	3.06	3.13	3.41	4.21	5.50	9.35	42.04	27.66	22.88	564.34	217.57	91.97
Zr	2.14	2.28	1.79	1.76	3.19	2.81	388.93	390.95	261.28	272.65	213	247.36
Nb	0.28	0.31	0.15	0.18	0.40	0.34	40.61	41.77	24.14	27.45	23.23	25.00
Mo	4.62	5.08	0.74	0.32	0.13	0.15	51.17	80.29	5.97	5.89	4.88	5.32
Cs	0.07	0.07	0.06	0.05	0.13	0.14	15.48	13.42	10.68	16.92	20.14	20.70
Ba	14.03	9.80	–	4.50	6.62	7.16	637.64	428.25	319.79	449.55	277.66	255.96
Hf	0.06	0.06	0.06	0.17	0.10	0.12	12.97	12.83	8.51	10.51	7.03	8.03
Ta	0.07	0.03	0.02	0.02	0.09	0.04	2.87	2.97	1.68	2.2	1.62	1.87
W	0.23	0.13	1.26	0.05	0.15	0.24	7.25	8.23	3.73	− 4.48	3.21	7.97
Pb	10.60	3.60	–	0.93	2.34	4.15	31.09	41.81	53.67	204.23	165.89	461.17
Th	0.24	0.27	0.13	0.13	0.23	0.24	14.73	12.20	10.46	35.24	29.18	34.22
U	0.31	0.34	0.51	0.25	0.30	0.33	8.91	11.31	4.93	10.33	7.06	10.93
Depth (cm)	725	675	650	625	610	600				590	589	584
ρ_w (g/cm^3)[c]		2.84	2.58							1.73	1.76	1.60
ρ_g(g/cm^3)			2.60		2.64					2.25	2.19	2.19
ϕ (%)			1							23	20	27

[a] Sample YT1, YT2 and YT3 stand for the acid-insoluble residues from samples Y1, Y2-2 and Y3-2, respectively, and others are the same as Fig. 2. Major and loss on ignition (LOI) values are in weight percent and trace elements values are in ppm.

[b] Chemical index of alteration (CIA) = $Al_2O_3/(Al_2O_3 + CaO^{\$} + Na_2O + K_2O)$, where $CaO^{\$}$ only represents the Ca in silicate (calculation with reference to Fedo et al., 1995; McLennan, 1993).

[c] The ρ_w, ρ_g and ϕ are bulk density, grain density and porosity, respectively.

the "soil rain" might spread over the study region. The vast Cenozoic (Early Pliocene to Late Holocene) volcanic rocks are distributed in the southwestern region of the Plateau, generally called the Tengchong Volcano Group (Zhu and Mao, 1983; The Qinghai-Tibet Plateau Scientific Investigation Team, 1989). All the above potential factors would affect the region of Guizhou Province. To sum up, the possible potential sources of soil developed on the karst terrains may be: the products of chemical weathering of carbonate rocks, Qua-

T4	T5	T6	T7	T8	T9	T10	T11	T12	T13	T14	T15	T16
35.56	32.21	37.13	33.76	34.07	33.72	34.53	35.52	31.63	35.84	34.18	34.97	34.44
0.72	0.75	0.72	0.99	0.94	0.89	0.92	0.82	0.80	0.94	0.87	0.80	0.92
29.58	33.16	31.92	32.91	33.40	31.73	32.44	31.54	34.37	31.49	35.19	34.54	33.64
9.64	9.72	11.32	11.51	10.02	10.75	11.12	12.80	14.02	10.00	13.83	11.92	11.01
0.76	1.48	0.98	0.79	1.18	1.55	1.18	0.10	0.08	1.12	0.07	0.08	0.75
0.39	0.10	0.06	0.03	0.02	0.03	0.03	0.03	0.03	0.03	0.03	0.02	0.03
1.30	0.90	0.80	0.82	0.90	0.80	0.80	0.70	0.60	0.60	0.60	0.70	0.90
0.41	0.50	0.50	0.20	0.21	0.20	0.10	0.20	0.20	0.11	0.01	0.01	0.20
0.45	0.58	0.45	0.39	0.59	0.31	0.40	0.42	0.39	0.21	0.43	0.52	0.42
3.49	2.09	1.50	1.62	1.52	1.55	1.48	1.37	1.51	1.62	1.52	1.62	1.73
0.18	0.36	0.15	0.30	0.12	0.27	0.12	0.01	0.03	0.15	0.01	0.15	0.13
16.84	17.50	14.10	16.20	17.00	18.01	16.05	16.06	16.01	17.40	12.85	13.90	15.21
99.32	99.35	99.63	99.52	99.97	99.81	99.17	99.57	99.67	99.51	99.59	99.23	99.38
86	91	92	94	92	94	94	93	93	94	94	94	93
71.19	63.56	63.44	50.16	50.68	55.64	49.74	48.35	50.57	50.17	50.73	51.43	50.77
231.11	287.69	294.11	292.78	295.22	327.98	306.12	295.25	306.42	288.85	283.62	299.40	299.37
125.21	141.47	142.75	139.83	141.09	158.91	147.59	143.01	150.89	141.24	138.86	141.28	145.42
155.58	105.94	59.92	27.57	25.88	29.04	26.77	25.34	26.75	26.91	26.71	33.73	31.77
294.51	168.65	158.81	124.58	127.68	139.99	129.22	120.48	126.97	124.49	123.34	130.11	128.43
191.46	168.16	158.93	143.35	146.35	162.87	153.28	139.91	161.00	140.88	144.22	137.21	141.56
589.30	356.50	364.86	296.45	291.98	324.70	297.68	285.78	299.55	283.24	276.98	287.95	290.60
42.18	47.07	45.93	45.82	47.31	51.29	46.38	46.21	45.33	43.04	44.24	48.05	47.76
170.60	129.33	104.10	111.66	113.88	121.17	114.21	112.27	111.22	112.93	108.89	123.51	127.12
71.01	68.67	60.22	65.49	63.28	69.28	67.47	67.70	70.33	74.73	73.86	71.41	74.41
36.38	28.69	29.95	28.11	28.41	32.24	29.44	28.39	34.93	30.32	28.18	27.76	27.59
285.76	265.37	235.59	256.09	254.88	272.32	252.66	252.32	257.08	264.31	260.29	258.66	274.06
26.66	26.58	24.08	27.45	26.87	28.56	26.99	26.45	27.40	28.68	28.72	28.96	29.15
6.84	6.09	4.99	4.74	5.15	5.72	4.95	4.74	4.90	4.44	4.37	7.10	5.15
20.53	22.32	21.26	24.28	24.15	26.47	23.99	24.69	24.62	23.26	22.55	24.56	25.29
320.65	243.12	190.23	216.56	215.50	229.99	211.03	211.34	205.36	228.78	227.32	243.50	251.28
9.60	8.54	7.55	8.56	8.56	8.86	8.53	8.37	8.25	8.12	8.58	8.66	8.54
1.92	1.85	1.67	2.02	1.96	2.16	1.95	1.91	2.00	2.24	2.03	2.12	2.21
3.61	3.61	3.13	3.73	3.65	4.29	3.64	3.46	3.61	3.75	3.68	3.82	3.90
367.62	181.95	114.32	80.30	72.48	88.17	74.95	77.78	81.63	70.80	82.36	85.10	83.03
34.38	34.45	33.17	35.18	36.56	38.10	36.29	35.42	37.69	36.97	36.62	37.65	238.46
9.41	9.88	9.31	8.98	8.45	9.64	9.18	8.91	9.40	9.33	9.46	9.55	9.75
574	563	553	543	533	523	513	503	493	483	473	463	453
1.62	1.43	1.45	1.58	1.38	1.77	1.66	1.49	1.45	1.41	1.74	1.61	1.61
			2.18			2.20						2.25
			28			25						28

(continued on next page)

ternary deposits, eolian loess accumulates and volcanic ashes, or their mixtures.

Although there is a widespread Cenozoic volcanic rock in southwestern region of the Plateau, volcanic ashes occur as limitedly distribution in the Plateau as pointed out by Zhao (1988). For example, there was no volcanic ashes found in Guizhou Province. Meanwhile, in the study of selected samples from the Pingba profile we have not observed primary volcanic minerals and volcanic

Table 1 (*continued*)

T17	T18	T19	T20	T21	T22	T23	T24	T25	T26	T27	T28
34.29	36.96	33.50	35.58	34.97	36.65	35.78	35.39	37.21	36.50	34.69	34.78
0.65	0.75	0.87	0.74	0.84	0.90	0.92	0.94	0.73	0.71	0.92	0.73
33.78	32.65	32.68	33.19	32.92	33.54	32.83	30.53	32.36	33.07	33.64	35.57
12.61	12.30	11.71	14.02	10.39	11.63	12.42	10.28	11.91	12.42	10.01	11.23
0.09	0.10	0.69	0.08	1.41	0.07	0.08	0.82	0.09	0.08	1.05	0.07
0.03	0.02	0.03	0.03	0.03	0.02	0.03	0.03	0.03	0.03	0.03	0.04
0.70	0.71	0.80	0.70	0.90	0.71	0.60	0.92	0.70	0.72	0.80	0.70
0.10	0.30	0.30	0.10	0.20	0.11	0.01	0.10	0.02	0.10	0.20	0.30
0.69	0.62	0.31	0.60	0.53	0.66	0.32	0.27	0.33	0.31	0.22	0.63
1.66	1.80	1.90	1.60	1.89	1.76	1.73	2.07	2.06	2.02	2.12	1.66
0.02	0.07	0.12	0.01	0.15	0.07	0.01	0.15	0.01	0.01	0.12	0.07
14.77	13.34	16.29	13.15	15.37	13.52	15.02	17.77	13.91	13.51	15.35	13.63
99.39	99.62	99.20	99.80	99.60	99.64	99.75	99.27	99.36	99.48	99.15	99.41
93	92	91	92	92	92	93	92	92	92	92	92
51.77	47.48	48.89	43.51	44.82	44.17	41.90	41.05	41.96	39.45	41.77	42.70
304.75	279.81	280.80	271.68	283.27	277.85	276.06	266.92	287.31	279.23	282.58	287.70
146.49	134.57	135.41	137.23	133.97	132.29	137.96	131.49	141.74	134.58	139.60	135.79
33.52	29.74	30.89	28.33	27.86	28.33	30.79	26.25	27.84	27.26	26.68	29.12
130.26	119.83	125.51	117.83	124.40	130.90	126.81	118.63	127.42	129.38	140.96	133.09
147.48	127.51	129.46	127.47	132.61	124.38	125.29	118.69	123.15	119.15	120.30	127.26
299.14	272.19	288.57	258.70	276.25	273.81	280.78	263.93	282.01	276.32	284.76	288.51
48.34	44.12	44.46	43.64	43.77	44.59	44.29	44.13	44.81	42.48	43.67	42.66
127.52	113.62	113.62	95.40	114.42	118.98	111.92	114.46	113.50	111.33	116.08	104.26
76.86	68.93	69.88	66.85	70.27	70.75	67.22	69.71	71.09	71.98	73.75	66.43
29.58	23.82	25.76	21.48	25.91	24.66	24.033	22.27	23.40	24.02	22.53	22.90
269.40	251.24	258.48	247.72	259.94	263.09	254.77	250.38	265.94	273.12	258.49	242.14
29.74	27.26	28.04	28.04	28.94	29.52	26.87	28.56	29.30	30.90	29.92	26.71
5.37	5.18	5.26	5.06	5.67	5.44	5.64	4.97	5.18	5.72	5.03	5.74
26.01	22.37	22.57	22.27	23.05	23.76	22.69	23.53	22.74	22.19	23.23	21.20
254.46	231.80	241.87	217.13	243.02	255.32	225.99	249.84	240.77	243.38	253.12	206.30
8.65	8.34	8.60	8.20	8.48	8.48	8.29	8.58	9.06	8.69	8.25	8.04
2.13	2.01	2.03	1.93	2.14	2.09	1.90	2.15	2.04	2.26	2.19	1.95
4.03	3.72	3.75	–	3.83	3.79	3.67	3.93	4.47	3.91	6.88	3.75
91.50	77.43	79.69	76.89	84.86	81.96	68.68	75.57	74.40	81.40	83.82	86.85
39.10	34.73	37.54	34.20	38.22	37.42	35.33	36.93	35.99	35.54	38.48	35.32
9.64	9.19	9.44	8.45	9.22	9.40	9.19	8.70	9.17	8.93	9.05	9.28
443	433	423	413	398	388	378	368	358	348	338	328
1.44	1.50	1.70	1.54	1.71	1.49	1.47	1.41	2.42	1.88	1.49	1.40
							2.27				
							38				

glass fragments, as well as secondary allophanite, immogolite and ferrihyrite that are typical of volcanic ashes. An et al. (1991) considered that southwest monsoon would influence only in the Weining region of western Guizhou Province (Fig. 1). Thus it is suggested that volcanic ashes from the Tengchong volcanic group are difficult to impact the central Guizhou Province that is mainly under the control of southeast monsoon. Moreover, the high mountains in west of the plateau (Fig. 1),

T29	T30	T31	T32	T33	T34	T35	T36	T37	T38	T39	T40
35.26	34.60	33.62	33.63	35.26	31.17	14.39	28.04	33.17	40.59	49.31	47.56
0.76	0.88	0.75	0.90	0.92	0.84	0.31	0.72	0.82	0.92	0.75	0.92
35.21	32.44	33.83	33.65	32.92	30.53	11.45	28.39	31.96	29.05	24.33	24.09
11.84	10.16	12.82	11.31	10.04	16.00	58.38	22.24	13.23	11.28	8.84	9.60
0.06	1.44	0.08	0.09	1.36	0.68	0.62	0.28	0.17	0.12	0.26	0.50
0.04	0.04	0.14	0.04	0.09	0.21	0.06	0.03	0.03	0.03	0.05	0.05
0.90	0.82	0.80	0.90	0.70	0.60	0.30	0.80	0.70	0.70	0.60	0.80
0.10	0.30	0.12	0.10	0.20	0.30	0.20	0.50	0.20	0.20	0.30	0.20
0.67	0.42	0.46	0.53	0.33	0.40	0.19	0.50	0.47	0.30	0.24	0.25
2.30	1.77	1.64	1.76	1.53	1.64	0.54	1.60	1.63	1.33	1.15	1.23
n.d	0.35	0.02	n.d	0.12	0.32	0.09	0.25	0.09	n.d	n.d	0.25
12.38	15.91	14.99	16.45	15.73	16.65	12.86	15.82	16.81	15.41	14.06	13.99
99.52	99.13	99.27	99.36	99.20	99.34	99.39	99.17	99.28	99.93	99.89	99.44
90	93	93	92	94	93	92	91	92	93	92	94
39.84	41.26	42.17	38.40	36.71	40.75	30.20	43.75	33.23	21.89	23.86	23.45
307.20	306.09	310.44	285.75	275.82	296.71	122.87	272.41	299.50	247.72	208.68	295.49
137.54	143.47	147.22	134.72	132.69	168.15	84.06	122.70	151.77	161.70	140.49	139.53
28.93	32.78	44.26	23.74	36.83	113.05	87.27	42.65	55.41	16.41	15.98	17.48
135.82	168.03	179.22	148.17	122.49	123.07	54.46	112.63	105.95	60.00	51.98	61.67
132.17	151.67	150.04	139.08	117.76	133.61	52.26	124.36	119.32	68.50	61.33	74.17
288.00	369.27	394.33	369.41	285.06	293.27	140.24	286.55	281.57	162.58	157.12	157.48
40.93	46.84	47.74	44.22	44.20	42.51	16.43	40.16	45.20	35.87	31.05	33.27
117.29	104.67	111.57	102.05	97.88	85.46	32.26	90.36	98.20	78.39	91.67	92.84
69.25	62.33	65.62	65.33	69.31	61.94	22.67	58.81	66.86	61.83	70.67	66.90
23.03	24.65	25.75	25.28	25.30	25.93	9.18	21.51	24.47	22.79	31.00	31.13
285.94	253.87	264.68	261.46	250.27	233.53	87.64	234.58	272.98	345.38	337.47	371.26
32.61	26.64	28.38	27.67	27.45	24.76	9.09	24.53	29.50	38.74	41.18	35.22
5.61	5.69	5.84	-	5.18	5.60	3.39	4.92	6.34	5.20	4.30	5.04
21.98	23.41	23.13	20.85	20.86	18.51	7.56	19.57	20.53	18.62	17.24	16.90
206.48	200.47	210.79	205.75	206.89	188.71	62.50	173.17	214.05	218.28	242.22	215.29
9.92	8.25	8.87	8.49	8.35	7.61	2.89	7.50	8.50	11.42	11.87	11.55
2.23	2.00	1.97	2.07	1.83	1.69	0.67	1.73	2.02	2.85	3.00	2.38
3.77	3.55	3.81	3.79	3.55	3.33	1.39	3.33	4.10	4.77	4.78	4.11
96.94	86.53	120.98	80.76	96.51	170.22	225.25	93.22	76.40	25.33	37.82	51.29
32.12	35.27	36.44	35.81	35.91	33.47	12.97	33.27	36.21	26.45	29.73	30.37
11.00	8.82	9.81	9.19	8.79	9.34	7.20	9.88	8.81	6.48	7.83	8.01
326	321	281	251	221	196	176	146	106	66	26	11
1.38	1.41	1.57	1.27	1.40	1.47	2.94	1.37	1.32	1.71	1.86	2.22
					2.20						2.26
					33						2

for example Mt. Gaoligong is also one of the important factors that prevent Tengchong volcanic ashes from drifting northeastwards. So the influence of volcanic ashes on this region can be basically excluded during Quaternary period.

3. Sampling and analytical methods

The Pingba profile (26°24′ N, 106°30′ E) discussed in this paper is located in the upland of karst terrain of central Guizhou Province and the upper reaches of Wujiang River (a southern tributary for Yangtze River) (Fig. 2), developed on gently dipping early–middle Triassic dolomites with about 1% acid-insoluble residues (Anshun formation, T1a, 712 m in total thickness). The profile is thick, with four horizons recognized in the field: the soil horizon (A-horizon, top for farming layer), the regolith horizon [B-horizon, can be subdivided into the red soil layer, ferruginous crust layer, reddish soil layer, yellow soil layer and chocolate layer (the soil layer's color is similar as that of chocolate)], the weathering bedrock horizon (can be subdivided into the flour dolomite layer, cracked dolomite layer and primary dolomite layer) and fresh bedrock horizon. Samples were collected from a shallow sampling well (man-dug holes) (Fig. 2).

The method to extract insoluble residues from dolomites for the samples (Nos. YT1 and YT2 in Table 1) was the same as the description of Wang et al. (1999). The new procedure of extracting insoluble residues from dolomites for samples (Nos. YT2-1 and YT3) differs mainly from the above method in non-pulverizing samples. A 250 g bulk sample prepared from the original rock was taken and placed into a 500 ml beaker, followed by the addition of super pure water and vibration of 30 min with supersonic wave, then the muddy liquid of the solution was dumped, once again samples were washed-up with super pure water and evaporated until dryness. Hydrochloric acid (1 N) was added to the dry samples and put aside for dissolution and settling until the leach solution became clean. The upper leach solution was pass through a filter paper. It was done repeatedly until all carbonate was dissolved completely. The residual sample was washed repeatedly with super pure water until the eluate became neutral, and evaporated until dryness (the filter paper was ignited to 800 °C in a crucible, and weighted). The detection results of X-ray diffraction showed that there exerted no difference in the mineral compositions of insoluble residues between the above two extracting procedures.

The air-dry bulk samples were finely ground in agate mortar into the experiment sizes (200 mesh) before analysis and dissolution. Bulk density (ρ_w) and grain density (ρ_g) of rock and soil samples were determined with the paraffin and hydrostatic pressure method, respectively. The porosity (ϕ) was calculated by the formula: $\phi = 1 - \rho_w/\rho_g$. The mineral composition was analyzed using X-ray diffraction (XRD) and the semiquantitative calculation of mineral composition was based on K value method (Schultz, 1964). Experimental apparatus is the Dmax/2200 model made by Japan, including the instrument standard CuKα target, 40 Kv, 20 mA, scanning scope for 2–60°, scanning step length for 0.04°, and scanning speed for 10°/min. Samples were placed on glass petrographic slides and then analyzed in the air-dried, ethylene alcohol at 300 and 550 °C treatment states for identification of hydroxy-interlayered vermiculite or chlorite, gibbsite, kaolinite and mix-layer mica/smectite. Kaolinite and halloysite were not discriminated in the quantitative XRD results.

The major elements were determined by wet chemical techniques, atomic absorption and flame photometry as a supplementary technique. The trace elements were analyzed using inductive-coupled plasma-mass spectroscopy (ICP-MS) techniques (ELEMENT, Finnigan MAT). The open vessel acid digestions method was used for the pretreatment of sample (Jarvis, 1992). Sample (0.1 g) was taken and put into a Teflon beaker, followed by addition of 1.5 ml HF and 1 ml HNO_3. The beaker was placed on a hot plate (~ 140 °C) for 48 h, until the sample was completely dissolved and vaporized to dryness. After that, 1 ml HNO_3 was added together with a proper amount of water, followed by heating so as to make all the salts dissolved completely. The resultant solution was placed into 50 ml plastic bottle and measured with In as the internal standard. All the analyses were monitored by using standard samples, and the analytical uncertainties involved in measurements are: ±5% for major elements, 10% for trace elements, <20%

for Sc, and <30% for Hf (see Appendix A). The above analyses and measurements were all accomplished at the Institute of Geochemistry, Chinese Academy of Sciences.

4. Results

4.1. Mineral composition of the red residua

The physical parameters and mineral compositions of the samples collected from the Pingba profile are shown in Fig. 3. The bulk density of samples generally displays a little variation in the regolith horizon ($\rho_w = 1.32-1.76$), with a significant change occurring mainly at the regolith–bedrock interface, which may be related to the huge volume change at the interface (named non-isovolumetric weathering). The bulk density tends to increase at the ferruginous crust and so does it in the top A-horizon. The porosity of the profile tends to increase upward, but an opposite trend is observed in the top A-horizon. The main mineral assemblages in the profile are: clay minerals + quartz + feldspar + iron oxides + anatase, and the clay

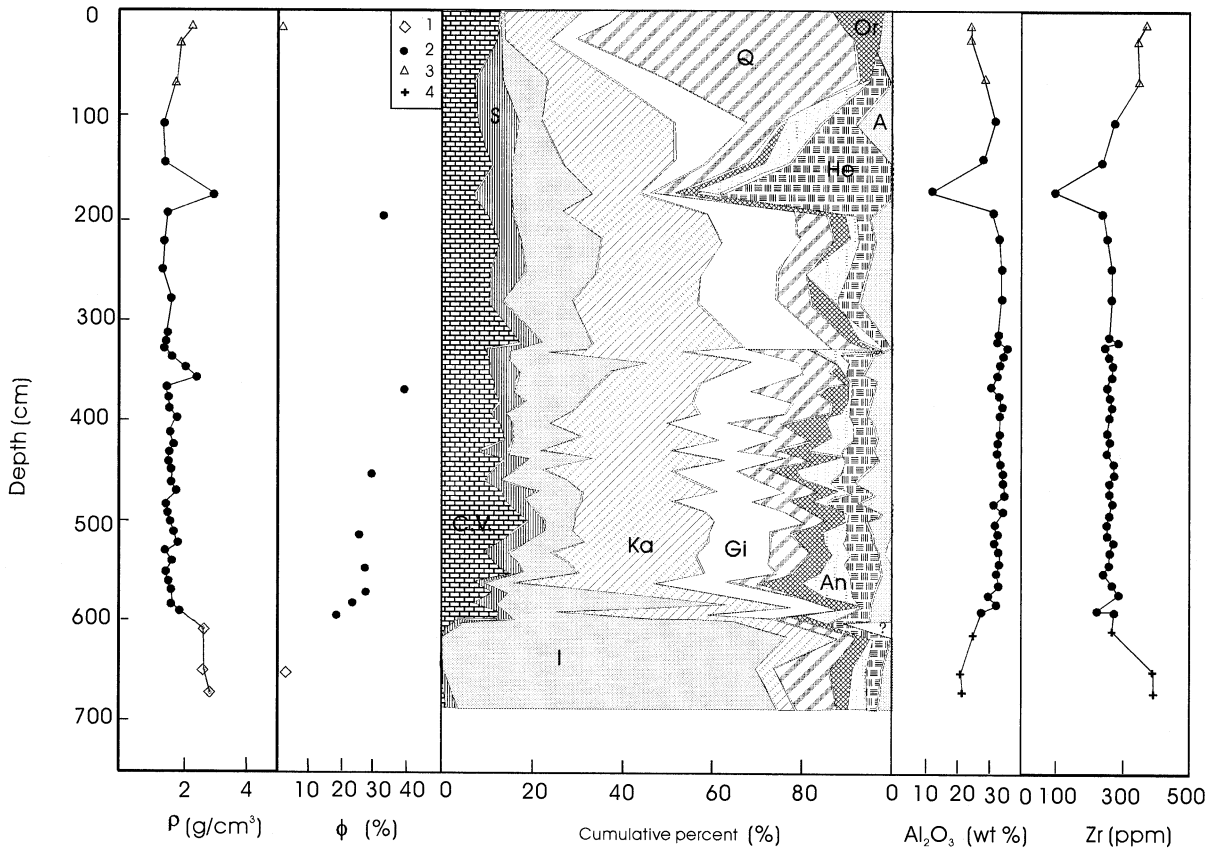

Fig. 3. Depth profiles of bulk density (ρ_w) and porosity (ϕ); mineralogical composition; Al_2O_3 and Zr concentration in the Pingba profile. The mineralogical distribution is calculated from X-ray diffraction data (vol.%) and includes the bulk porosity, but does not include amorphous mineral. Mineral abbreviations: C.V. = hydroxy-interlayered vermiculite or chlorite, I = illite, Ka = kaolinite, Gi = gibbsite; S = smectite, Or = K-feldspar, An = plagioclase, He = iron minerals (in regolith for iron oxides, including hematite and goethite; in bedrock horizon for pyrite), A = anatase. The legends of 1, 2, 3 and 4 represent samples in the bedrock horizon (sample numbers: HY ~ Y3-2), the regolith horizon (sample numbers: T1 ~ T37), the soil horizon (sample numbers: T38 ~ T40) and the insoluble residues from dolomite (sample numbers:YT1 ~ YT3), respectively.

minerals are composed of illite + kaolinite + gibbsite + smectite + hydroxy-interlayered minerals of vermiculite or chlorite, and both hematite and goethite are identified as iron oxides (Fig. 3). Only in sample T1 (chocolate layer) from B-horizon appears amphibole mineral (the peak with $2\theta = 10.56$, i.e., $d = 8.3705$ in the XRD patterns; with the largest contents accounting for about 8.8% of the total minerals). Meanwhile, the mineral composition of the insoluble residues is dominated by illite, accounting for more than 70%, with quartz, feldspar, kaolinite, pyrite and anatase coming next. Minor amounts of chlorite and smectite are recognized in bedrocks except for flour dolomite sample. As compared to the clay minerals from the regolith with from the bedrock horizon, the former appear gibbsite minerals and the contents of primary illite minerals decrease whereas those of kaolinite minerals increase, but the total amount of clay minerals generally maintains less change in whole profile (Fig. 3). The bedrock contains primary pyrite, but it has been transformed into secondary goethite and hematite in the regolith. The contents of clay minerals tend to decrease in the A-horizon above the pedogenic interface. Even illite and other clay minerals disappear in the top layer; however, the contents of quartz show a drastic increase.

4.2. Chemical composition of the red residua

The chemical compositions of the samples from the Pingba profile are listed in Table 1. High LOI of samples reflects the influence of high water-bearing phases (mainly clay minerals) and organic matter in the profile. The major elements show a trend of homogeneous variation in the B-horizon, with the exception of the ferruginous crust layer. The contents

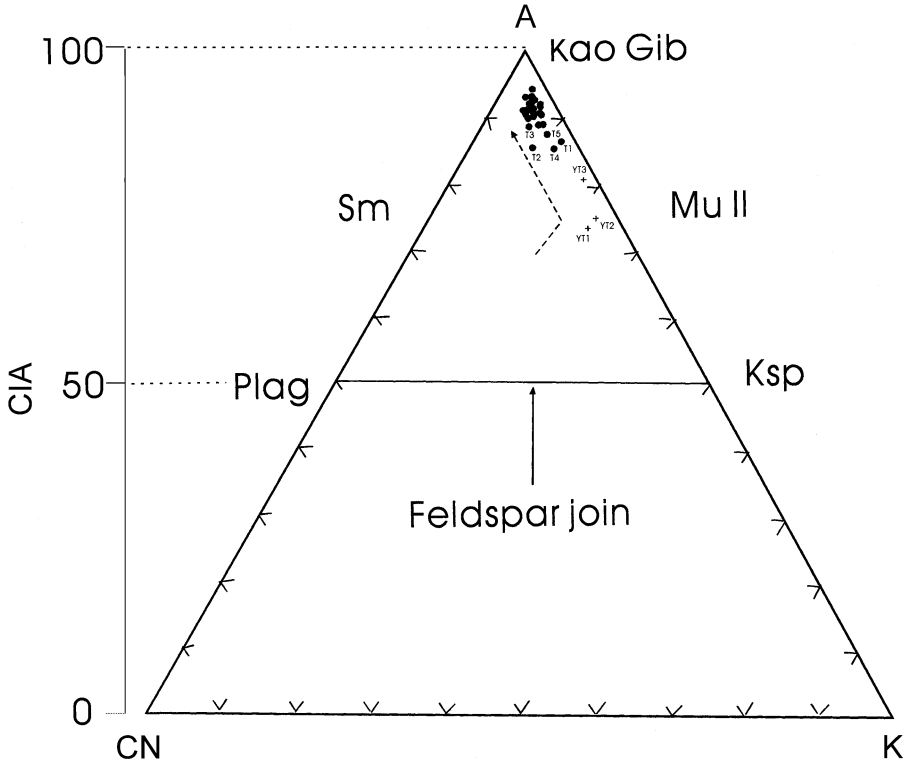

Fig. 4. Basic Al_2O_3-CaO*+ Na_2O-K_2O (A-CN-K) ternary phase diagram for samples from the Pingba profile. Dotted line represent the weathering trend (after Fedo et al., 1997). Mineral abbreviations: Kao = kaolinite, Gib = gibbsite; Mu = muscovite; Il = illite Ksp = K-feldspar; Plag = plagioclase (entire series); Sm = smectite.

of SiO_2 and Al_2O_3 are generally identical, 32–37 and 32–34.5 wt.%, respectively. The contents of SiO_2 and Al_2O_3 in the ferruginous crust layer are estimated to be 14.39 and 11.45 wt.%, respectively, and those of Fe_2O_3 are up to 58.38 wt.%. As compared to samples from the B-horizon with the A-horizon, the latter tend to increase and decrease the contents of SiO_2 and Al_2O_3, respectively. The chemical index of alteration (CIA) (see Nesbitt and Young, 1982) for the profile varies from 84 to 94, with an obvious variation in the lower B-horizon and no remarkable variation from the above regolith–bedrock interface to the top of the profile (Table 1). In the Al_2O_3-CaO* + Na_2O-K_2O (A-CN-K) triangular diagram (where CaO* represents Ca in the silicate fraction only) (Fig. 4), the samples cannot be notably distinguished and almost all the samples are close together to the joint A-K. Insoluble residues are close to the area where illite or muscovite lies, and the other samples occur near the point A from the lower to upper part of the profile.

An average upper continental crust (UCC)-normalized spiderdiagram for the samples from the Pingba profile is shown in Fig. 5. Dolomite samples and their insoluble residues both show similar element distribution patterns, with the exception of the element Sr which shows an opposite distribution pattern (Fig. 5A). The insoluble residues are characterized by remarkable depletion in Sr, Na and precise enrichment in Mo relative to UCC. The UCC-normalized spiderdiagram of all the samples from the B-horizon and A-horizon (Fig. 5B) show similar element distribution features as those of insoluble residues. Sample T35 from the ferruginous crust also has similar element distribution characteristics (except that the total amount of the elements is slightly lower). As compared with the insoluble residues, the samples from

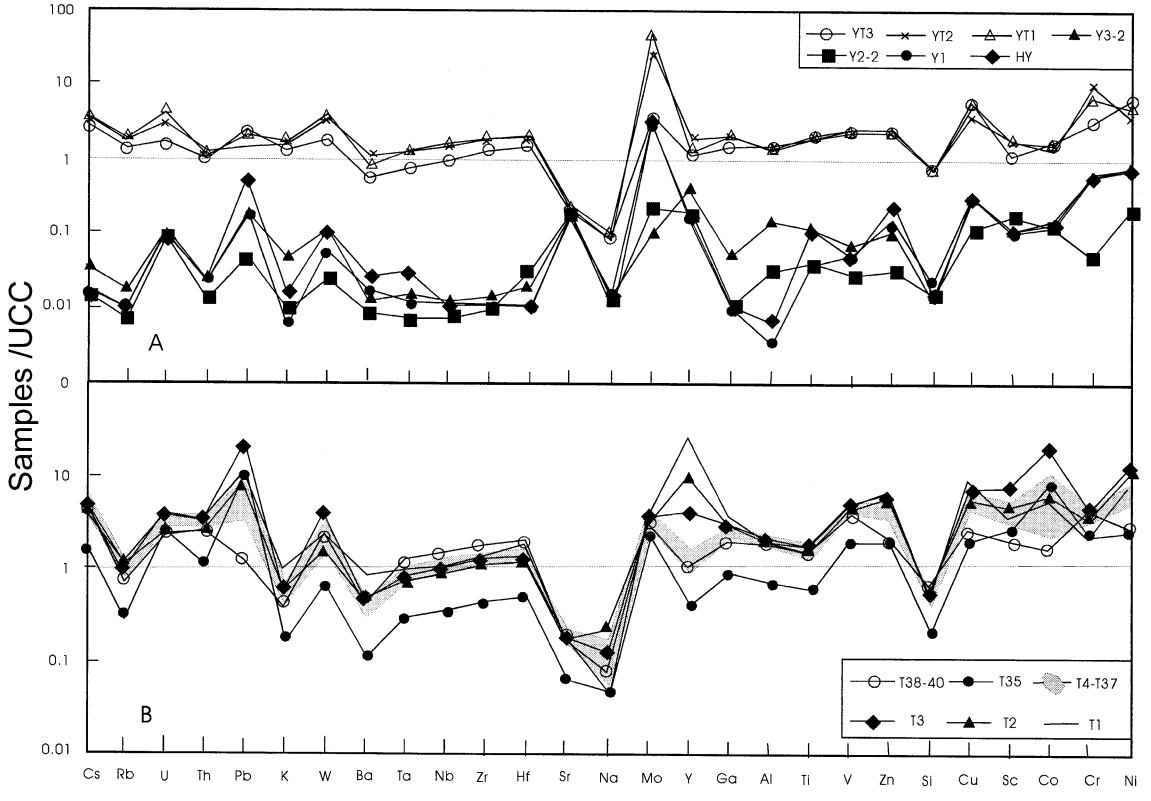

Fig. 5. UCC-normalized spiderdiagrams for samples from the Pingba profile. (A) Dolomites and their acid-insoluble residues. (B) Samples in A- and B-horizons of the profile. The UCC values are from Taylor and McLennan (1985). The element order follows Hofmann (1988) and is determined by the order of decreasing normalized concentration of the upper continental crust as referred to the primitive mantel, with few exceptions. The regularity of these patterns demonstrates the homogeneity of the source.

the B-horizon are characterized by enrichment in Pb and Co and depletion in Ba, K, Rb, Si and Cr. Samples T1, T2 and T3 from the lower B-horizon are all characterized by an abnormal enrichment of the element Y. Samples from the A-horizon have slightly lower contents of Pb, Sc, Cu and Co than those from the B-horizon.

5. Discussion

5.1. The geochemical criteria for in situ weathering

Investigations of modern soil profiles have revealed that allochthonous components would be carried by wind and water into the upper part of the profile (Schellmann, 1989; Maynard, 1992). And the components are usually enriched in SiO_2, Al_2O_3, TiO_2 and Zr (Condie et al., 1995). In the Pingba profile, the contents of less mobile elements such as Al_2O_3 and Zr are fairly homogenous throughout the profile and only show variations at the regolith–bedrock interface and at the ferruginous crust (Fig. 3). The former fact implies that the profile is formed from a unified source without any exotic materials incorporated into it, and the latter resulted from a large variation in volume at the interface and the ferruginous crust layer (as verified by the distribution of bulk densities in Fig. 3). The contents of Al_2O_3 are found to decrease accompanying with increase for those of Zr at the top of the profile. This may be directly related to the leaching-induced loss of the Al-bearing clay minerals and the increase of clastic minerals in the A-horizon (Fig. 3). Or it may be attributed to the export of more mobile elements than Zr during chemical weathering (Kirkwood and Nesbitt, 1991).

The elements Al, Ti and Fe are the less mobile elements during chemical weathering, but their geochemical behaviors are different. For instance, the solubility of iron is controlled by oxidation–reduction, but the case is not true for Al and Ti, whose solubilities are controlled mainly by pH value. At pH = 4–10 and 2–14 the hydroxides of Al and Ti are insoluble, respectively, and Al^{3+} and Ti^{4+} in the soil solution precipitate or occur in clay minerals in the form of oxide and hydroxide. The relationship between Al_2O_3 and TiO_2 is shown in Fig. 6A. There is a positive correlation for the dolomite samples and samples from the B-horizon ($R^2 = 0.87$). The above characteristics indicate that the Pingba profile is a typical one of in situ weathering (see Young and Nesbitt, 1998). Samples from the A-horizon and the insoluble residues distributed over the range of extreme weathering (i.e., Ti/Al ratio increase), probably owing to the physical migration of the Al-rich phase (e.g., clay minerals) or to the migration of Al as a result of chemical dissolution (Maynard, 1992; Young and Nesbitt, 1998). It is implied that the process of extracting insoluble residues from the dolomite by 1 N hydrochloric acid is similar to the pedogenesis that occurred at the top of the profile. The relationship between Al_2O_3 and Fe_2O_3 is shown in Fig. 6B. The samples from the ferruginous crust layer and two samples from the upper and lower layers show a very good correlation ($R^2 = 0.99$); other samples also have a good correlation ($R^2 = 0.94$). Al and Fe in the Pingba profile share the same geochemical behavior (immobile) which implies that the profile possesses the characteristics of in situ weathering.

5.2. Quantification of soil sources by mineralogy and geochemistry

5.2.1. Mineralogical evidences

Whether eolian fine-grained materials are involved or not is one of the key factors in the study of the genesis of soils and the formation mechanism of weathering profiles in karst terrain. The clay minerals in the Pingba profile are generally equivalent to those of "insoluble residues" in the dolomites (Fig. 3), and gibbsite is a distinguished mineral surveyed only in the regolith. Gibbsite is commonly considered to form in laterites, especially in the uplands of moist tropical and subtropical zones (Hus, 1989). The climatic condition in Guizhou Province makes it reliable to form gibbsite. The mineral assemblages in the Pingba profile are very similar to those in Terra Rossa of the western Sicily, Italy (Bellanca et al., 1996). The main origin hypotheses for the Terra Rossa, either the intense weathering of carbonate rocks in subtropical and tropical climates or a product of important eolian contributions, or both are considered. However, total contents of clays are of less change in the vertical in the Pingba profile, which may have not shown if there is addition of eolian clay minerals. Loss of some clay minerals in the upper part of the profile has been found in A-horizon, which

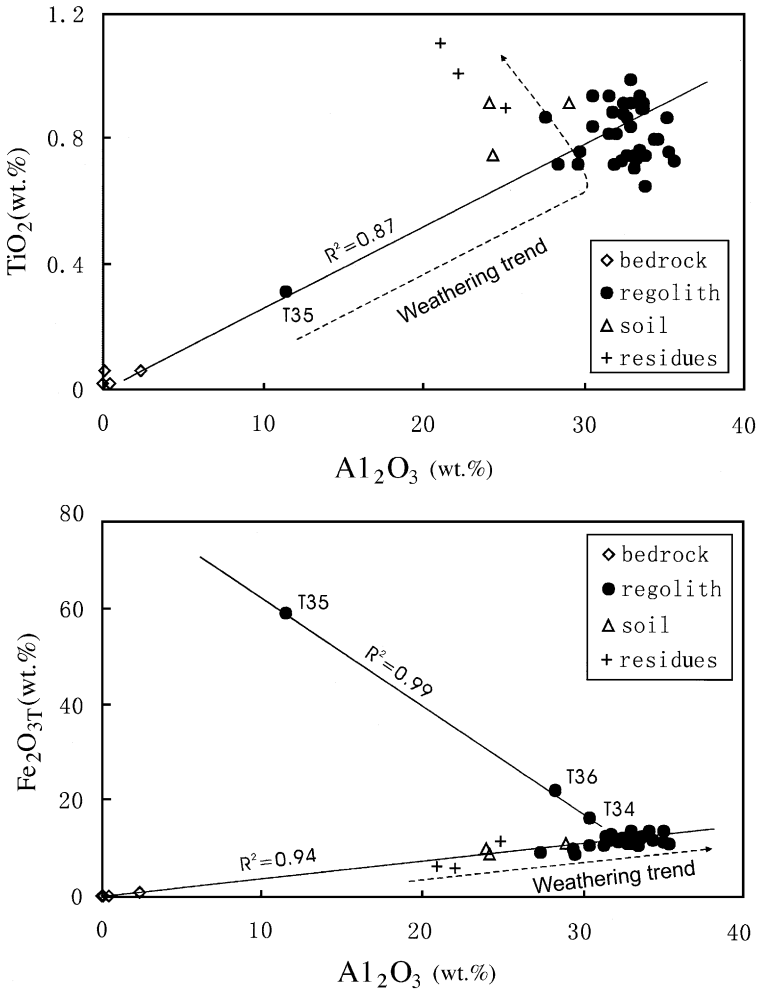

Fig. 6. The distribution of TiO_2 and Al_2O_3 in the Pingba profile. (A). Distribution of Ti/Al ratios in the profile. (B). Al_2O_3 vs. Fe_2O_{3T} in the profile. See text for detailed explanation. The legends of bedrock, regolith, soil and residues represent the samples in the bedrock horizon, the regolith horizon, the soil horizon and the insoluble residues from dolomite, respectively.

consists of the fact that the contents of clay minerals decrease from the bottom to the top in many weathering profiles (Kraus, 1997). The mineral compositions of the Pingba profile reflect a distinctive inheritance between the insoluble residues in the dolomite and the overlying red residua, and there is no evidence of incorporation of exotic components.

5.2.2. Major and trace element evidences

As viewed from the distribution of the major elements in samples from the B-horizon and A-horizon in the Pingba profile, they have higher Al_2O_3 contents and CIA values (Table 1) and show some difference from the pelitic rocks, which have high Al_2O_2 contents, moderate CIA values and low CaO and Na_2O concentrations (Cullers et al., 1997). As shown in the A-CN-K diagram (Fig. 4), samples from the lower part of the profile (especially those from the insoluble residues of the dolomite and above the regolith–bedrock interface) are distributed along the joint A-K and tend to approach to the A end, reflecting a process in which K_2O is leached out and Al_2O_3

is increased in the samples, i.e., the dissolution of feldspar and illite minerals and the production of new clay minerals (gibbsite and kaolinite). The SiO_2/Al_2O_3 ratios in the samples from B-horizon are less variable and low (≈ 1), but their K_2O/Na_2O ratios vary considerably in the range of 2–18 (Fig. 7). The above ratios are quite different from those of PAAS, UCC and Chinese loess. The SiO_2/Al_2O_3 ratios in samples from A-horizon and the insoluble residues are higher than those of samples from B-horizon (Fig. 7), and the ratios of sample T1 from the bottom of B-horizon are within the same range as those of the insoluble residues in the dolomite. The major element data indicate that almost no exotic components have been incorporated into the Pingba profile. Meanwhile, they also show that samples from this profile are different from those from the sediments and loess sources.

The dolomite and its insoluble residues share much in common with respect to trace element distribution patterns (Fig. 5); only the element Sr shows a different situation. It is indicated that many trace elements in the dolomite are controlled primarily by those of its insoluble residues. Because Sr is partly contained in the lattice of dolomites, Sr distribution in the dolomite and its insoluble residues are different. As compared with values of UCC, Sr and Na in the insoluble residues are more depleted because they are mobile during weathering (Nesbitt et al., 1980). Mo in the dolomite is more enriched because it is of marine sedimentary origin (e.g., Dean et al., 1999). The trace element distributions of samples from the B-horizon are very similar to those of the insoluble residues (Fig. 5), suggesting a pronounced inheritance from the insoluble residues. Compared with the insoluble residues, samples from the B-horizon are enriched in Pb and Co and depleted in Ba, K, Rb, Si and Cr, which is directly related to the continuous dissolution of illite and feldspar minerals, the formation of new clay minerals (gibbsite, kaolinite), and an increase in oxidation intensity in the profile during chemical weathering from the bedrock to the residue horizon. Pb and Co can be dissolved in the acidic oxidizing environment but precipitated in the alkaline reducing environment (Liu et al., 1984). It is probable that Pb and Co are greatly depleted in the extraction of insoluble residues from the dolomite by way of acid leaching. K, Rb and Ba dominate in K-feldspar, illite and kaolinite (Plank and Langmuir, 1998) and have similar behavior in

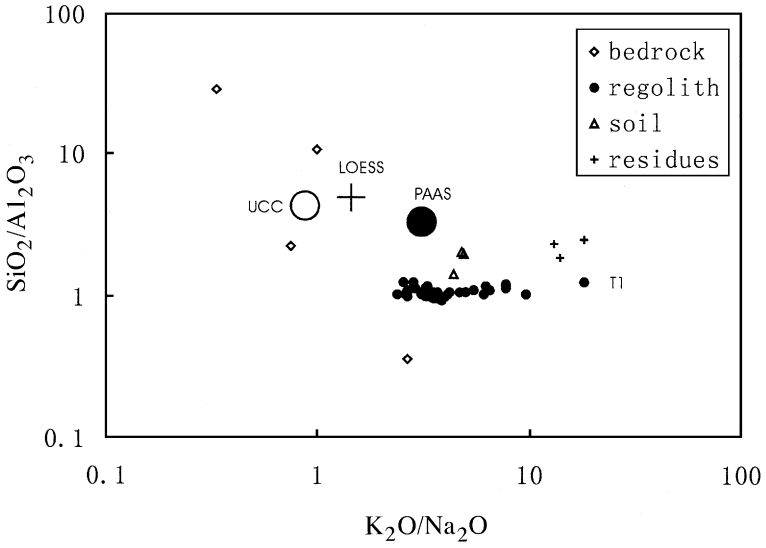

Fig. 7. Plot of SiO_2/Al_2O_3 vs. K_2O/Na_2O for Pingba profile. Upper continental crust (UCC) and Post-Archean average Australian shale (PAAS) values used here are from Taylor and McLennan (1985), and Chinese loess (LOESS) values used are from Gallet et al. (1996), respectively. For symbols see Fig. 6.

the weathering profile, which are influenced by the solubility of the host minerals K-feldspar or illite. Si is mobile during chemical weathering, so the depletion of Si can be recognized in the B-horizon. The distribution of Cr is controlled by oxidation–reduction (Middelburg et al., 1988). Soluble $HCrO^{-}_{4}$ may occur in the strongly oxidizing environment (Van der Weijden and Reith, 1982), hence leading to a decrease in Cr in the B-horizon. Unusual enrichment of Y is recognized in samples from lower B-horizon. That is because REE minerals are enriched in the samples or Y is not an immobile element during weathering (White, 1995; Nesbitt and Markovics, 1997). The distribution of the trace elements demonstrated that there is a pronounced inheritance between bedrock and residual soils and the above descriptions lend great support to the cognate relation between the dolomite and its overlying regolith.

5.2.3. Elemental ratio evidences

In soil solution the elements Ca, Na, K, Mg, Mn and Si are highly soluble and can be preferentially exported from the soil profile while the element Al would be retained in the soil profile because it is less mobile and tends to be concentrated in typical weathering products such as clay minerals and oxides (Chesworth et al., 1981; Middelburg et al., 1988). For this reason, some people made use of Si/Al ratio as an index of weathering intensity (Birkeland, 1984; Muhs et al., 1987, 1990; Borg and Banner, 1996). For example, the ratio Si/Al is relatively small in the strongly weathered soil. The ratios of Ca/Al, Mg/Al, Na./Al, Mn/Al and K/Al usually decrease upwards in the vertical weathering profile that is formed in situ from a homogenous parent rock. Fig. 8 shows the vertical variation trend of the ratios of mobile to immobile elements in the Pingba profile. There is a drastic decrease in Si/Al ratio in the profile at the

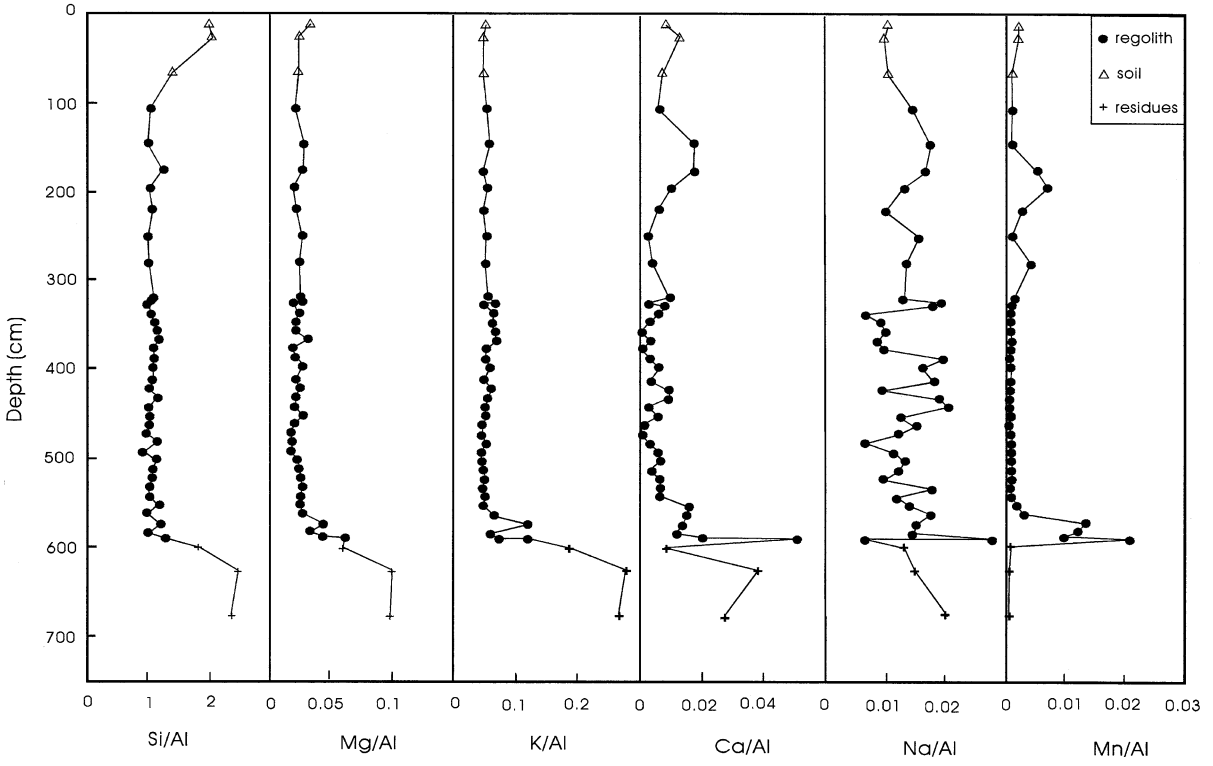

Fig. 8. Depth profiles of Si/Al, Mg/Al, K/Al, Ca/Al, Na/Al and Mn/Al ratios in bulk samples of the Pingba profile. The element ratios in bedrock horizon are from those in insoluble residues in the dolomites. For symbols see Fig. 6.

weathering bedrock horizon, but the ratio is less variable at B-horizon. The results are in good consistence with those obtained in terms of CIA (Table 1). There appears an increase in Si/Al ratio in A-horizon of the profile, which may be not caused by the decrease of weathering intensity; but instead it is attributed to a result of leaching-induced loss of Al-rich clay minerals in large amounts and the increase of quartz minerals (Fig. 3). As shown in Fig. 8, the ratios of Mg/Al, K/Al, Ca/Al and Na/Al are precisely decreased in the weathering bedrock and regolith horizon, whose variation trend is similar to that of Si/Al ratio, reflecting that transport of mobile elements in the initial stage of dolomite weathering would lead to the separation of Al from alkali metals and alkaline earth metals. The aforementioned characteristics suggest that plagioclase minerals in the lower part of the profile have altered into clay minerals during progressive weathering and as a result of Na, Ca and Mg are preferentially leached out (Nesbitt et al., 1980) and Mg is also involved in the formation of secondary minerals such as smectite, vermiculite or illite, these secondary minerals will remain in the profile (Middelburg et al., 1988). These reasons lead to the decrease of Mg/Al, Ca/Al and Na/Al in the lower profile and no remarkable variation in Mg/Al ratio in the upper profile. Except for the Mn/Al ratio, there is a drastic increase in the lower regolith and the ferruginous crust layer; the ratios of K/Al and Mn/Al remain considerably constant through the regolith (Fig. 8). K/Al ratio reflects the extent of alteration of feldspar into clay, no obvious variation in this ratio because K-feldspar is more resistant against weathering than plagioclase or further reflects K preferentially adsorbed on clays (White et al., 1996). So, K is immobile relative to Na and Ca. Mn is an indicator for oxidation–reduction (Middelburg et al., 1988). Manganese (II) released during weathering will be oxidized to Mn (IV) and precipitate, resulting in its enrichment, i.e., the increase of Mn/Al ratio in the lower regolith and the ferruginous crust layer. No obvious variation in Mn/Al ratio at the weathering bedrock horizon may reflect that Mn-bearing minerals are less variation in the process.

Whether the constant ratios of immobile elements are consistent with those of the weathered phase in the underlying bedrocks can be used as one of the important indices to distinguish weathering profile from sedimentary rock (Rye and Holland, 1998). Because immobile elements including Al, Ti, Zr and Nb still maintain relatively constant in the soil environment or under the most strongly weathering conditions (Schwarz, 1997), i.e., the ratios of element pairs such as Al/Zr, Ti/Zr and Ti/Nb in the weathered samples are usually equivalent to those of parent rocks if the weathering profiles formed from the completely homogenous parent rocks. However, the ratios of immobile element pairs remain constant in a few cases for sediments in the vertical profile. Fig. 9 shows the vertical variation trend of immobile elements in the Pingba profile. Al/Zr, Ti/Zr and Ti/Nb ratios are very slight in both the bedrock horizon and the B-horizon, except for the ratio of Al/Zr in B-horizon (Al/Zr = 0.101–0.139) which is slightly higher than that in ''insoluble residues'' in the dolomite (Al/Zr = 0.054–0.096), and it does not support the conclusion of allochthonous contributions in the profile because the deviation of Al/Zr is less than 40% from flour dolomite to the regolith (deviation=$(Al/Zr_{soil} - Al/Zr_{parent})/Al/Zr_{parent}$, Maynard, 1992). The ratios of Al/Zr, Ti/Zr and Ti/Nb in the A-horizon decrease to some extent as compared with those in the B-horizon. This may be related to the leaching-induced loss of Al-rich clay minerals in the soil horizons mentioned above and the loss of Ti at the top of the weathering profile. The above results indicate that the Pingba profile is the product of chemical weathering rather than that of sedimentary materials.

5.3. Geochemical processes for formation of the red residua

5.3.1. Major elements behavior within the red residua

The samples from the A-horizon are significantly different from those from the B-horizon in the Pingba profile (Fig. 10A–C), the former being high in SiO_2 and TiO_2 and low in Al_2O_3 and K_2O contents. Major elements of samples from the profile are also precisely different from values of PAAS, UCC and Chinese loess. An actual leaching-accumulating trend has been approved among samples of the dolomites and their insoluble residues (Fig. 10A–C), because the latter is a result of extracting experiment from the formers in this study. The sample T35 from the ferruginous crust layer is also distributed on the middle segment of the trend (Fig. 10A,B). A possible weathering trend has also

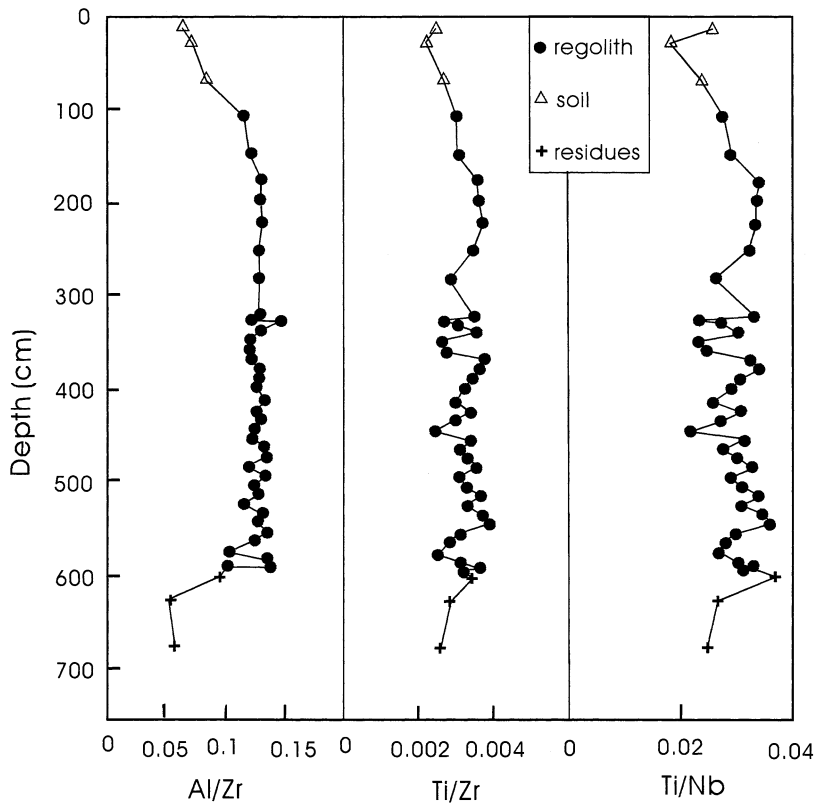

Fig. 9. Depth profiles of Al/Zr, Ti/Zr and Ti/Nb ratios in bulk samples of the Pingba profile. The element ratios in bedrock horizon are from those in insoluble residues in the dolomites. For symbols see Fig. 6.

been suggested in the insoluble residues and samples from the lower B-horizon, which are corresponding to 'the decrease in SiO_2 and constancy in TiO_2' (Fig. 10A), 'the decrease in SiO_2 and increase in Al_2O_3' (Fig. 10B) and 'the decrease in K_2O and increase in Al_2O_3' (Fig. 9C), respectively. They consist of the stages divided in chemical weathering processes of some red residua in southern China, for instance the "Al-enrichment and Si-depletion" and the "Al-enrichment and K-depletion" stage (Xi, 1991). In Fig. 10A,B the compositional variables of samples from A-horizon is similar to those of the insoluble residues, reflecting a leaching process once experienced by the A-horizon and it is similar to the process of extracting insoluble residues from the dolomite. This lends support to a conclusion that the pedogenesis may be a kind of leaching process (Chen et al., 1996). However, the compositional variables of samples from A-horizon is different from those of insoluble residues in Fig. 10C, i.e., samples from A-horizon and those from the top of B-horizon constitute a straight line with no variation in K_2O and a decrease in Al_2O_3, which is consistent with "Al-depletion" for the highest stage of red residua development (Zhao and Shi, 1983).

5.3.2. High field strength elements (HFSE) and the formation of red residua

Braun et al. (1990) have confirmed that Th is an immobile element in red residue profiles; however, the leaching may lead to the export of U from the weathered or altered profiles (i.e., the weathering process tends to oxidize insoluble U^{4+} to soluble U^{6+}), therefore, Th/U ratios tend to increase in the red residue profiles. Pb is normally concentrated in feldspar minerals, especially in K-feldspar (Fung and Shaw, 1978). With the destruction of feldspar minerals in a weather-

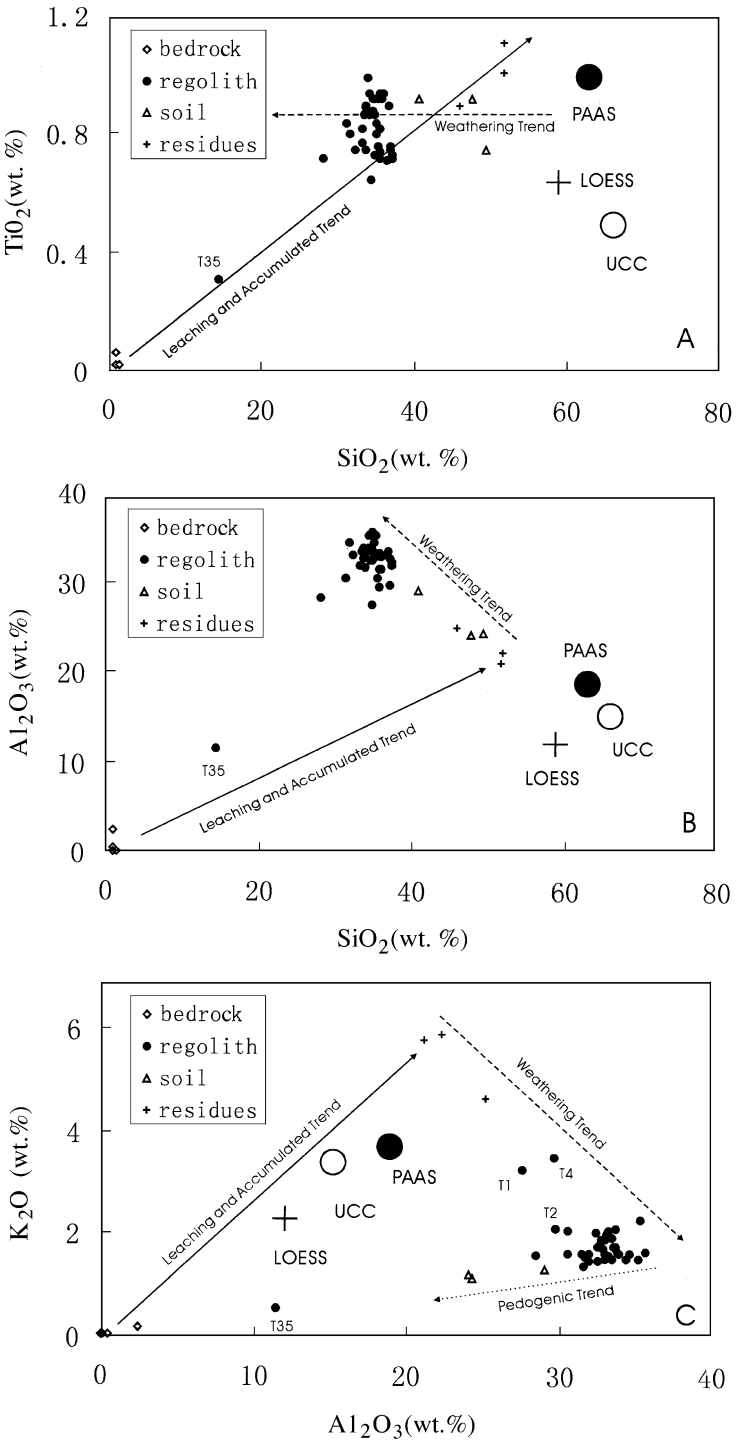

Fig. 10. (A) TiO_2 vs. SiO_2, (B) Al_2O_3 vs. SiO_2 and (C) K_2O vs. Al_2O_3 diagrams comparing samples from the Pingba profile with UCC, PAAS and Chinese loess. The values of UCC, PAAS and LOESS described as in Fig. 7. For symbols, see Fig. 6.

ing profile, Pb will remain into newly formed clay minerals in the profile. The samples from B-horizon in the Pingba profile are distributed mainly around the line of UCC (Th/U = 3.8) and they are consistent with the chemical weathering trend ($R^2 = 0.53$) as defined by McLennan et al. (1995), with ratio Th/U (Th/U = 2.92–4.33) increasing progressively (Fig. 11A). An actual leaching-accumulating trend ($R^2 = 0.65$) is obtained between dolomite samples and their insoluble residues in Fig. 11A, and the sample from the ferruginous crust layer is also distributed on the trend. Meanwhile, a weathering trend with the ratio Th/U = 1.6 has been observed among insoluble residues ($R^2 = 0.66$, the samples from ferruginous crust layer and the lower B-horizon are near the trend) (Fig. 11B). The samples from B-horizon form the weathering trend with the ratio Th/U = 4.4 ($R^2 = 0.96$), and the samples from A-horizon are also distributed on this trend line (Fig. 11B). However, the ratios of Th/Pb and U/Pb in samples from A-horizon are higher than those of samples from B-horizon and the upper crust (UCC) (Fig. 11B). It is obvious that the Th/U ratio can reflect the extent of weathering for the samples in the profile. Th and U in the dolomites (Th/U = 0.5) have been influenced by a weak chemical weathering and the host fractions are the same for them in the process from primary dolomite through cracked dolomite to flour dolomite, but in B-horizon they have experienced the

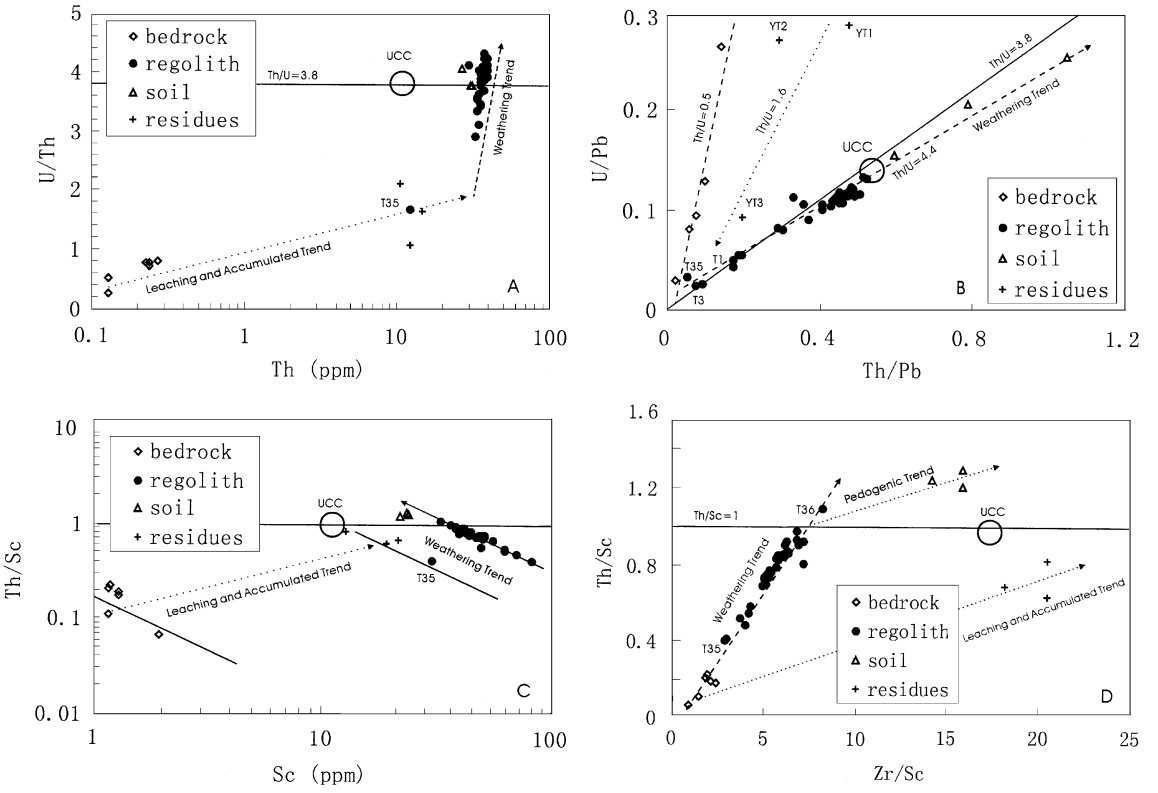

Fig. 11. (A) Th/U ratios vs. Th abundances, (B) Th/Pb vs. U/Pb ratios, (C) Th/Sc ratio vs. Sc abundances and (D) Th/Sc ratios vs. Zr/Sc ratios for bulk samples from the Pingba profile. Solid line is defined by the UCC (Taylor and McLennan, 1985). Long dotted line indicates the weathering trend in this study, except in map A which is after McLennan et al. (1995) and in map D which is similar to the primary compositional trend defined by Condie (1993) for average Phanerozoic rock compositions. Short dotted line indicates the leaching-accumulating trend during the dolomite weathering as matter of fact. For symbols see Fig. 6.

process of increase weathering intensity that is identical as indicated with CIA values. Higher Th/Pb and U/Pb ratios in samples from A-horizon may be attributed to the export of Pb from clays owing to the effects of leaching rather than an extent of weathering increase from B-horizon to A-horizon in the profile. A decrease in the ratios of Th/Pb and U/Pb in the insoluble residues has been noticed during dolomite weathering from primary dolomite to flour dolomite (Fig. 11B). This may be ascribed to the progressive enrichment of feldspar minerals in the residues.

The element Sc has relatively low abundance in natural waters and is related with Fe during weathering processes (e.g., Dennen and Anderson, 1962). And it is more concentrated in clays in soils (Cullers, 1988). However, the element Zr is a typical immobile element for it is low in solubility and usually concentrated in highly weathering-resistant zircon in supergenic environments (Milnes and Fitzpatrick, 1989). As can be seen in Fig. 11C, the data of the samples from A-horizon are more than the typical value of UCC (Th/Sc = 1), but those of the samples from the B-horizon are almost lower than this value. And the latter are distributed mainly on a trend with ratio Th/Sc ranging from 0.41 to 1.09, and increasing upward the B-horizon. It represents a chemical weathering trend line because the line is in parallel to the weathering trend bounded by dolomite samples and their insoluble residues (including sample from the ferruginous crust layer) and different from the mixing line defined by Fedo et al. (1997). In Fig. 11D dolomite samples and B-horizon samples constitute a positive correlation line ($R^2 = 0.96$), a continuous increasing of Th/Sc and Zr/Sc ratios. The line is similar to a primary compositional trend defined by average Phanerozoic rock compositions from Condie (1993). And it is indicative of the process for leaching-induced loss of clays with Sc during weathering, namely a weathering trend. A trend line constituted by samples from the top of B-horizon and those from A-horizon is in parallel to the actual leaching-accumulating trend between dolomite samples and their insoluble residues, reflecting that pedogenesis at top the profile is obviously affected by leaching processes and the profile is a typical weathered profile. Therefore, it is also shown that the formation of red residua involves two stages, i.e., leaching-accumulating (residual soils) and re-evolution of the residual soils, thereby lending great support to our previous results (Wang et al., 1999; Ji et al., 2000).

5.3.3. Evolution model for the soil profile

Under different physical and chemical conditions, vertical zonings were formed in various layers of red residua that some given geochemical processes could be inverse deduced by the regularity of elements, including distribution, transport and fractionation. Some researchers put forward three-stage evolution for red residua underlying carbonate rocks (Wei et al., 1983; Zhou and Chen, 1994), for example, the early cracked, middle granulated and late rubified stages. But those stages are difficult to be distinguished from each other using field and experimental data. Others described the main weathering features of the red residua on a large spatial and temporal background (geomorphic features), e.g., two-stage model for karst landscape development (e.g., Twidale, 2001 and references therein; Li et al., 2002). However, the two-stage model was well available for chemical weathering of the red residua on a microsystem scale, for instance, two stage evolution of red residua developed on carbonate rocks from mineralogical and geochemical data was suggested by Wang et al. (1999). According to the geochemical evidences for the red residua presented in this paper, two-stage characteristics can be made a clear distinction for evolution of the profile (e.g., Figs. 10 and 11). The major process of weathering crust evolution occurs in the transition from the first to the second one, for example, many parameters have occurred change in the periods from rock to soil and the chocolate layer (Table 1), and some geochemical processes discussed above appear similar to those from lateritic profiles in southern China (e.g., Fig. 10). Chemical composition change is not very obvious for the profile at the second stage (e.g., Figs. 4 and 7). Those evolution characteristics of red residua developed on karst terrains are incompletely similar to those for the other weathering crusts. It may have been a unique quality for the development of red residua on karst terrains.

From the above paragraph and from element distribution diagrams (e.g., Figs. 10 and 11), we

see that samples from the ferruginous crust are often distributed on the weathering trend or near the leaching-accumulating trend. The genesis of in situ weathering and the leaching processes have been suggested for its formation. As shown in Fig. 6B, the elements Al and Fe become notably negatively correlative in the ferruginization and rubification processes, probably indicating that aluminium is transported downward and the iron was accumulated in the place during the regolith reduction. The results support the conclusion that the indurated iron crust forms in warm and moist climate with wet and dry alternating environmental condition (Nahon, 1986; Tardy et al., 1991; Beauvais and Colin, 1993; Tardy, 1997). It develops at depth in soil profiles during warm humid periods as iron is leached from the overlying soils and incorporated into secondary minerals at depth, and would uplift to the surface when soil erosion happens during ensuing dry periods. At the same time, we pay attention to samples from the soil layer that are clearly different from those from the regolith in many element diagrams (e.g., (Figs. 6, 7, 10 and 11)). They distribute commonly together with insoluble residues or parallel to the leaching-accumulating trend (e.g., Fig. 11D), demonstrating that leaching process has also an important meaning for the formation of soils in this study.

6. Conclusions

This study has revealed material sources of the Pingba red residua developed on the Triassic dolomite on the Yunnan-Guizhou Plateau and its formation mechanism. Mineral composition and elemental chemical data had fully verified that the Pingba profile was formed as a product of in situ weathering. The elemental distributions in the profile were mainly controlled by the process of accumulation and evolution of "insoluble" constituents in the dolomites, e.g., the continuous dissolution of illite and feldspar minerals, the formation of new clay minerals (gibbsite, kaolinite) and the increase of oxidizing intensity in the profile. Meanwhile, the results of this study led to support the hypotheses of two-stage formation mechanism for the Pingba red residua, e.g., the first stage for the leaching of carbonate rocks and accumulation of insoluble residues on karst terrains (forming residue soils) and the second one for the chemical weathering of the residue soils. Among them, the major process for red residua evolution occurs in the transition period from the first to the second stage, and the chemical composition change for the profile is not very obvious at the second stage. It is also suggested the insoluble residues from underlying Triassic dolomites as the parent materials for the red residua.

Through study on elemental geochemistry characteristics for the sample from the ferruginous crust layer, such a conclusion that the ferruginous crust is the product of in situ weathering dolomites under warm–humid subtropical climate condition has been suggested, and a leaching process has been noticed for the genesis of the ferruginous crust and soil layers in this study. In a word, this study has set up a typical example to solve formation mechanism of clay-rich soils in the carbonate rock district of the southern China.

Acknowledgements

The authors are most grateful to Profs. A.F. White, L.M. Walter and an anonymous referee for their helpful insights, which contributed to an obvious improvement of the manuscript. Special thanks to Prof. A.F. White, editor Mr. T. Horscroft, Associate Prof. W. Sui (Jilin Univ.) and Dr. C. Zhou are expressed here for correcting English writing. We thank Prof. Y. Qiu (Institute of Geochemistry, CAS) for providing standard samples and reference values in laboratory, S. Li for major elements analysis, G. Gong for XRD analysis, L. Dong and J. Pong for leaching experiments, and L. Qi for his assistance with ICP-MS. Furthermore, we are indebted to Profs. Y. Chen and L. Zhou (Peking University) for discussion and suggestion about this study. This work was jointly supported by the knowledge-renovation Project of Chinese Academy of Sciences (KZCX2-105), the National Natural Science Foundation of China (NSFC) grants (No. 49833002 and 40243020), the Postdoctoral Foundation of China, the CAS K.C. Wong Postdoctoral Research Award Fund, and the "Western Light" Program sponsored by the Chinese Academy of Sciences. **[LW]**

Appendix A. ICP-MS analyses of the blanks and international reference standards and those of repeatedly determined samples both in China and in other countries (unit: ppm)

	NBS-1633a	Recommended value	RSD (%)	JB-1a	Recommended value	RSD (%)	C4CH	C4CH reference value*	RSD (%)	Blank (ppb)	Detection limit (ppb)
Sc	40.08	40	0.2	32.11	27.9	15.1	22.13	18.6 ± 0.2	18.9	0.12	0.12
V	303.16	297	2.1	210.22	220	− 4.4	124.43			0.231	0.033
Cr	198.83	196	1.4	405.34	415	− 2.3	116.18	110 ± 2	5.6		0.42
Co	45.48	46	− 1.1	38.80	39.5	− 1.8	21.88	19.7 ± 0.2	11.1	0.1	0.018
Ni	134.88	127	6.2	148.80	140	6.3	34.17	27 ± 13	25.9	0.885	0.16
Cu	122.04	118	3.4	50.71	55.5	− 8.6	36.68			2.17	0.37
Zn	220.96	210	5.2	89.18	82	8.7	24.78			5.237	0.66
Ga	59.44	58	2.5	18.09	18	0.5	27.97			0.035	0.026
Rb	127.22	131	− 2.9	39.03	41	− 4.8	208.50	196 ± 4	6.4	0.025	0.036
Sr	901.61	830	8.6	452.82	443	2.2	44.89	43 ± 11	4.4	1.12	0.11
Y	84.07	86	− 2.2	23.29	24	− 3.0	26.17			0.003	0.022
Zr	246.72	232	6.3	150.17	146	2.9	104.07	100 ± 20	4.1	0.049	0.010
Nb	30.95	30	3.2	28.95	27	7.2	13.67			0.085	0.005
Mo	29.89	29	3.1	1.37	1.4	− 2.1	0.19			0.045	0.061
Cs	10.55	10.42	1.3	1.21	1.2	0.8	5.87			0.001	0.001
Ba	1275.75	1320	− 3.4	468.74	468.74	− 5.7	402.34	399 ± 11	0.84	5.501	0.087
Hf	7.83	7.29	7.4	7.83	3.48	23.3	3.50	2.78 ± 0.04	25.9	0.012	0.003
Ta	2.05	1.93	6.2	1.76	2	− 12.0	0.87	0.809 ± 0.017	7.54	0.003	0.0007
W	4.53	4.6	− 1.5	2.41			1.03			0.005	0.008
Pb	75.86	72.4	4.8							2.521	0.067
Th	24.50	24.7	− 0.8	9.19	8.8	4.4	13.69	12.0 ± 0.2	14.1	0.008	0.003
U	9.91	10.2	− 2.8	1.69	1.6	5.6	1.95	1.92 ± 0.10	1.6	0.005	0.0008

Sample number NBS-1633a and JB-1a represent coal fly ash and basalt samples from National Institute of Science and Technology (NIST) and Geological Survey of Japan (GSJ), respectively; C4CH is a sample collected from Chuanlinggou shale in the Yuxian section, Hebei province, China; the reference values were measured by Prof. Randy Korotev of the Washington University in St. Louis (the sample and reference values are provided by Prof. Qiu Yuzhuo).

* Shows different the references values with the recommended values.

References

Ahmad, N., Jones, R.L., 1969. Genesis, chemical properties and mineralogy of limestone-derived soils, Barbados, west Indies. Trop. Agric. 46, 1–15.

Ahmad, N., Jones, R.L., Beavers, A.H., 1966. Genesis, mineralogy of west Indian soils: I. Bauxitic soils of Jamaica. Proc. - Soil Sci. Soc. Am. 30, 719–722.

An, Z.S., Wu, X.H., Wang, P.X.et al., , 1991. Changes in the monsoon and associated environmental changes in China since the last interglacial. In: Liu, T.S. (Ed.), Loess, Environment and Global Change. Science in China Press, Beijing, pp. 1–29.

Aubert, D., Stille, P., Probst, A., 2001. REE fractionation during granite weathering and removal by waters and suspended loads: Sr and Nd isotopic evidence. Geochim. Cosmochim. Acta 65, 387–406.

Banfield, J.F., Eggleton, R.A., 1989. Apatite replacement and rare earth mobilization, fractionation, and fixation during weathering. Clay Clay Miner. 37, 113–127.

Beauvais, A., Colin, F., 1993. Formation and transformation processes of iron duricrust systems in tropical humid environment. Chem. Geol. 106, 77–101.

Bellanca, A., Hauser, S., Neri, R., Palumbo, B., 1996. Mineralogy and geochemistry of Terra Rossa soils, western Sicily: insights into heavy metal fractionation and mobility. Sci. Total Environ. 139, 57–67.

Berg, G., 1932. Das Vokommen der chemischen Elementen auf der Erde. Johann Ambrosius Barth, Leipzig, p. 204.

Berner, R.A., 1995. Chemical weathering and its effect on atmospheric CO_2 and climate. In: White, A.F., Brantley, S.L. (Eds.), Chemical Weathering Rates of Silicate Minerals. Rev. Mineral, vol. 31, pp. 565–582.

Birkeland, P.W., 1984. Soil and Geomorphology. Oxford Press.

Blatt, H., Middleto, G.V., Murray, R.C., 1980. Origin of Sedimentary Rocks. Prentice-Hall, Englewood Cliffs, NJ, p. 782.

Borg, L.E., Banner, J.L., 1996. Neodymium and strontium isotopic constraints on soil sources in Barbados, West Indies. Geochim. Cosmochim. Acta 60, 4193–4206.

Braun, J.-J., Pagel, M., Muller, J.-P., Bilong, P., Michard, A., Cuillet,

B., 1990. Cerium anomalies in lateritic profiles. Geochim. Cosmochim. Acta 54, 781–795.

Braun, J.-J., Viers, J., Dupre, B., Polve, M., Ndam, J., Muller, J.-P., 1998. Solid/liquid REE fractionation in the lateritic system of Goyoum, East Cameroon: the implication for the present dynamics of the soil covers of the humid tropical regions. Geochim. Cosmochim. Acta 62, 273–299.

Brimhall, G.H., 1988. Metal enrichment in bauxites by deposition of chemically mature Eolian dust. Nature 333, 819–824.

Ceng, Z., 1958. Preliminary study on red soil topography in districts of South China. The Collection of Physical Geography Articles in South China. The Commercial Press, Beijing, pp. 35–48. In Chinese.

Chen, J., Wang, H.T., Lu, H.X., 1996. Study on trace elements and REE for loess through chemical leaching in Luochuan profile, Shanxi province, China. Acta Geol. Sin. 70, 61–71 (in Chinese).

Chesworth, W., Dejou, J., Larroque, P., 1981. The weathering of basalt and relative mobilities of the major elements at Belbex, France. Geochim. Cosmochim. Acta 45, 1235–1243.

Chubb, L.J., 1963. Bauxite genesis in Jamaica. Econ. Geol. 58, 286–289.

Clarke, O.M., 1966. The formation of bauxite on karst topography in Eufaula district, Labama, and Jamaica. Econ. Geol. 61, 903–916.

Comer, J.B., 1974. Genesis of Jamaican bauxite. Econ. Geol. 69, 1251–1264.

Condie, K.C., 1993. Chemical composition and evolution of the upper continental crust: contrasting results from surface samples and shales. Chem. Geol. 104, 1–37.

Condie, K.C., Dengate, J., Cullers, R.L., 1995. Behavior of rare earth elements in a paleoweathering profile on granodiorite in the Front Range, Colorado, USA. Geochim. Cosmochim. Acta 59, 279–294.

Cullers, R.L., 1988. Mineralogical and chemical changes of the soil and stream sediment formed by intense weathering of the Danburg granite, Georgia, USA. Lithos 21, 301–314.

Cullers, R.L., Bock, B., Guidotti, C., 1997. Elemental distributions an neodymium isotopic compositions of Silurian metasediments, western Maine, USA: redistribution of the rare earth elements. Geochim. Cosmochim. Acta 61, 1847–1861.

Dean, W.E., Piper, D.Z., Perterson, L.C., 1999. Molybdenum accumulation in Cariaco basin sediment over the past 24k.y.: a record of water-column anoxia and climate. Geology 27, 507–510.

Dennen, W.H., Anderson, P.J., 1962. Chemical changes in incipient rock weathering. Geol. Soc. Amer. Bull. 73, 375–383.

Drever, J.I., 1997. Weathering processes. In: Saether, O.L., Caritat, P.D. (Eds.), Geochemical Processes, Weathering and Groundwater Recharge in Catchments. A.A. Balkema, Rotterdam, pp. 3–19.

Drever, J.I., Clow, D.W., 1995. Weathering rates in catchments. In: White, A.F., Brantley, S.L. (Eds.), Chemical Weathering Rates of Silicate Minerals. Rev. Mineral, vol. 31, pp. 463–485.

Fedo, C.M., Nesbitt, H.W., Young, G.M., 1995. Unraveling the effects of potassium metasomatism in sedimentary rocks and paleosols, with implications for paleoweathering conditions and provenance. Geology 23, 921–924.

Fedo, C.M., Young, G.M., Nesbitt, H.W., 1997. Paleoclimatic contral on the composition of the paleoproterozoic serpent formation, huronian supergroup, Canada: a greenhouse to icehouse transition. Precambrian Research 86, 201–223.

Fung, P.C., Shaw, D.M., 1978. Na, Rb, and Tl distributions between phlogopite and sanidine by direct synthesis in a common vapour phase. Geochim. Cosmochim. Acta 56, 899–909.

Gallet, S., Jahn, B., Torii, M., 1996. Geochemical characterization of the Luochuan loess-paleosol sequences, China and paleoclimatic implications. Chem. Geol. 139, 67–88.

Gallet, S., Jahn, B., Lanoe, B.V.V., Dia, A., Rossello, E., 1998. Loess geochemistry and its implications for particle origin and composition of the upper continental crust. Earth Planet. Sci. Lett. 156, 157–172.

Guizhou Provincial Geological Survey Team (Ed.), 1995. Dictionary of Stratigraphic Terms of Guizhou, Guizhou Science and Technology Press, Guiyang, p. 30. In Chinese.

Hofmann, A.W., 1998. Chemical differentiation of the Earth: the relationship between mantle, continental crust, and oceanic crust. Earth Planet. Sci. Lett. 90, 297–314.

Huang, Z., 1996. Red Weathering Crust in Southern China. Ocean Press, Beijing, p. 228. In Chinese.

Hus, P.H., 1989. Aluminum oxides and oxyhydroxides. In: Dixon, J.B., Weed, S.B. (Eds.), Minerals in Soil Environment. Soil Science Society of American, Madison.

Isphording, W.C., 1978. Mineralogical and physical properties of Gulf Coast limestone soils. Trans. - Gulf Coast Assoc. Geol. Soc. 28, 201–214.

Jahn, B., Gallet, S., Han, J., 2001. Geochemistry of the Xining, Xifeng and Jixian profiles, loess plateau of China: aeolian dust provenance and paleosol evolution during the last 140 ka. Chem. Geol. 178, 71–94.

Jarvis, I., 1992. Sample preparation for ICP-MS. In: Jarvis, K.E., Gray, A.L., Houk, R.S. (Eds.), Handbook of Inductively Coupled Plasma Mass Spectrometry. Blackie, Glasgow, p. 229.

Ji, H.B., Ouyang, Z.Y., Wang, S.J., Zhou, D.Q., 2000. Element geochemistry of weathering profile of dolomitite and its implications for the average chemical composition of the upper-continental crust. Science in China (Ser. D) 43, 23–35.

Kirkwood, D.E., Nesbitt, H.W., 1991. Formation and evolution of soils from an acidified watershed: Plastic Lake, Ontario, Canada. Geochim. Cosmochim. Acta 55, 1295–1308.

Kraus, M.J., 1997. Lower Eocene alluvial paleosols: pedogenic development, stratigraphic relationships, and paleosol/landscape associations. Palaeogeogr. Palaeoclimatol. Palaeoecol. 129, 387–406.

Lasage, A.C., 1984. Chemical kinetics of water–rock interactions. J. Geophys. Res. 89, 4009–4025.

Legros, J.P., 1992. Soil of Alpine mountains. In: Martini, I.P., Chesworth, W. (Eds.), Weathering, Soil and Palaeosols. Elsevier, Amsterdam, pp. 155–181.

Li, D., Cui, Z., Liu, G., 2000. Features and origin of covered karst on Hunan, Guangxi, Guizhou, Yunnan and Tibet. J. Mt. Sci. 18, 289–295 (in Chinese).

Li, D., Cui, Z., Liu, G., 2002. A development model of red weathering crust on limestones: an example from Hunan, Guangxi, Guizhou, Yunnan and Tibet. Acta Geogr. Sin. 57, 293–300.

Lin, S.J., Zhou, Q.Y., Chen, P.Y., 1994. The Late Cenozoic Group

in Guizhou Province. Guizhou Science and Technology Press, Guiyang, p. 152. In Chinese.
Liu, Y.J., Cao, L.M., Li, Z.L., 1984. Element Geochemistry. Science in China Press, Beijing, p. 548. In Chinese.
Liu, T.S., et al., 1985. Loesses and environment Science in China Press, Beijing, p. 481.
Macfarlane, A.W., Danielson, A., Holland, H.D., Jacobsen, S.B., 1994. REE chemistry and Sm–Nd systematics of late Archean weathering profiles in the Fortescue Group, Western Australia. Geochim. Cosmochim. Acta 58, 1777–1794.
Marsh, J.S., 1991. REE fractionation and Ce anomalies in weathered Karoo dolerite. Chem. Geol. 90, 189–194.
Maynard, J.B., 1992. Chemistry of modern soils as a guide to interpreting Precambrian paleosols. J. Geol. 100, 279–289.
McLennan, S.M., 1993. Weathering and global denudation. J. Geol. 101, 295–303.
McLennan, S.M., Hemming, S.R., Taylor, S.R., Eriksson, K.A., 1995. Early Proterozoic crustal evolution: geochemical and Nd–Pb isotopic evidence from metasedimentary rocks, southwestern North American. Geochim. Cosmochim. Acta 59, 1153–1177.
Middelburg, J.J., Van Der Weijden, C.H., Woittiez, J.R.W., 1988. Chemical processes affecting the mobility of major, minor and trace elements during weathering of granitic rocks. Chem. Geol. 68, 253–273.
Milnes, A.R., Fitzpatrick, R.W., 1989. Titanium and zirconium minerals. In: Dixon, J.B., Weed, S.W. (Eds.), Minerals in the Soil Environment. Soil Science Society of America, pp. 1131–1205.
Monroe, W.H., 1986. Examples of the replacement of limestone by clay. Miss. Geol. 7, 1–6.
Muhs, D.R., Crittenden, R.C., Rosholt, J.N., Bush, C.A., Stewart, K.C., 1987. Genesis of marine terrace soils, Barbados, west Indies: evidence from mineralogy and geochemistry. Earth Surf. Processes Landf. 12, 605–618.
Muhs, D.R., Bush, C.A., Stewart, K.C., 1990. Geochemical evidence of Saharan dust parent material for soils developed on quaternary limestones of Caribbean and Western Atlantic Islands. Quat. Res. 33, 157–177.
Nahon, D., 1986. Evolution of iron crusts in tropical landscapes. In: Coleman, S.M., Detheir, P.D. (Eds.), Rates of Chemical Weathering of Rocks and Minerals. Academic Press, New York, pp. 275–282.
Nesbitt, H.W., 1979. Mobility and fractionation of rare earth elements during weathering of a granodiorite. Nature 279, 206–210.
Nesbitt, H.W., Markovics, G., 1997. Weathering of granodioritic crust, long-term storage of elements in weathering profiles and petrogenesis of silicclastic sediments. Geochim. Cosmochim. Acta 61, 1653–1670.
Nesbitt, H.W., Young, G.M., 1982. Early Proterozoic climates and plate motions inferred from major chemistry of lutites. Nature 299, 715–717.
Nesbitt, H.W., Markovics, G., Price, R.C., 1980. Chemical processes affecting alkalis and alkaline earths during continental weathering. Geochim. Cosmochim. Acta 44, 1659–1666.
Panahi, A., Young, G.M., Rainbird, R.H., 2000. Behavior of major and trace elements (including REE) during Paleoproterozoic pedogenesis and diagenetic alteration of an Archean granite near Ville Marie, Quebec, Canada. Geochim. Cosmochim. Acta 64, 2199–2220.
Plank, T., Langmuir, C.H., 1998. The chemical composition of subducting sediment and its consequences for the crust and mantle. Chem. Geol. 145, 325–394.
Plummer, L.N., Parkhurst, D.L., Wigley, T.M.L., 1979. Critical review of the kinetics of calcite dissolution and precipitation. ACS Symp. Ser. 93, 537–573.
Prospero, J.M., 1981. Eolian transport to the world ocean. In: Emiliani, C. (Ed.), The Oceanic Lithosphere. The Sea, vol. 7. Wiley, New York, pp. 801–874.
Rye, R., Holland, H.D., 1998. Paleosols and the evolution of atmospheric oxygen: a critical review. Am. J. Sci. 298, 621–672.
Schellmann, W., 1989. Allochthonous surface alteration of Ni-laterites. Chem. Geol. 74, 351–365.
Schultz, L.G., 1964. Quantitative interpretation of mineralogical composition from X-ray chemical data for the Pierre shale. U. S. Geol. Surv. Prof. Pap. 391-C, 31.
Schwarz, T., 1997. Distribution and genesis of bauxite on the Mambilla Plateau, SE Nigeria. Appl. Geochem. 12, 119–131.
Sharma, A., Rajamani, V., 2000a. Weathering of gneissic rocks in the upper reaches of Cauvery river, south India: implications to neotectonics of the region. Chem. Geol. 166, 203–223.
Sharma, A., Rajamani, V., 2000b. Major element, REE, and other trace element behavior in amphibolite weathering under semiarid conditions in southern India. J. Geol. 108, 487–496.
Stallard, R.F., 1995. Relating chemical and physical erosion. In: White, A.F., Brantley, S.L. (Eds.), Chemical Weathering Rates of Silicate Minerals. Rev. Mineral, vol. 31, pp. 543–564.
Sui, S., Yao, X., 2000. Quaternary red earth stratigraphy in southern China. Quat. Sci. 20, 182–185 (in Chinese).
Tardy, Y., 1997. Petrology of Laterites and Tropical Soils. A.A. Balkema, Rotterdam, p. 408 (translated by V.A.K. Sarma from pétrologiedes latérites et des sols tropicaux).
Tardy, Y., Kobilsek, B., Paquet, H., 1991. Mineralogical composition and geographical distribution of African and Brazilian periatlantic laterites. The influence of continental drift and tropical paleoclimates during the past 150 million years and implications for India and Australia. J. Afr. Earth Sci. 12, 283–295.
Taylor, S.R., McLennan, S.M., 1985. The Continental Crust: its composition and evolution. Blackwell Scientific Publication, Oxford, p. 311.
Teilhard de Chardin, P., Young, C.C., Pei, W.C., Chang, H.C., 1935. On the Cenozoic formations of Kwangsi and Kwangtung. Bull. Geol. Soc. China 14, 179–205.
The Qinghai-Tibet Plateau Scientific Investigation Team, 1989. The Tengchong Geothermal Field. Science Press, Beijing, p. 210. In Chinese.
Twidale, C.R., 2001. The two-stage concept of landform and landscape development involving etching: origin, development and implications of an idea. Earth-Sci. Rev. 57, 37–74.
Van der Weijden, C.H., Reith, M., 1982. Chromium(III)-chromium (VI) interconversions in seawater. Mar. Chem. 11, 565–572.
Wang, S.J., Ji, H.B., Ouyang, Z.Y., Zhou, D.Q., Zheng, L.P., Li, T.Y.,

1999. Preliminary study on weathering and pedogenesis of carbonate rock. Sci. China (Ser. D) 42, 572–581 (in Chinese).

Wei, Q.F., Chen, H.Z., Wu, Z.D., 1983. The geochemical characteristics of red lime soil (terra rossa) in Nonggang natural protect districts, Guangxi province. Acta Pedol. Sin. 20, 30–41 (in Chinese).

White, A.F., 1995. Chemical weathering rates of silicate minerals soils. In: White, A.F., Brantley, S.L. (Eds.), Chemical weathering rates of silicate minerals. Rev. Mineral, vol. 31, pp. 407–461.

White, A.F., Blum, A.E., Schulz, M.S., Bullen, T.D., Harden, J.W., Peterson, M.L., 1996. Chemical weathering rates of a soil chronosequence on granitic alluvium: I. Quantification of mineralogical and surface area changes and calculation of primary silicate reaction rates. Geochim. Cosmochim. Acta 60, 2533–2550.

White, A.F., Blum, A.E., Schulz, M.S., Vivit, D.V., Stonestrom, D.A., Larsen, M., Murphy, S.F., Eberl, D., 1998. Chemical weathering in a tropical watershed, Luquillo Mountains, Puerto Rico: I. Long-term versus short-term weathering fluxes. Geochim. Cosmochim. Acta 62, 209–226.

Xi, C., 1965. Several problems of China's weathering crust. Quat. Res. China 4, 42–54 (in Chinese).

Xi, C., 1990. Soils are long-term records of climate change. Acta Pedologica Sinica 1, 82–89 (in Chinese).

Xi, C., 1991. The discussion on weathering crust in the southern China. Quat. Sci. 1, 1–7 (in Chinese).

Yen, Q. (Ed.), 1983. China's Red Soils. Science in China Press, Beijing, p. 210. In Chinese.

Young, G.M., Nesbitt, H.W., 1998. Processes controlling the distribution of Ti and Al in weathering profiles, siliciclastic sediments and sedimentary rocks. J. Sediment. Res. 68, 448–455.

Young, C.C., Bien, M.N., Lee, Y.Y., 1938. "Red beds" of human. Bull. Geol. Soc. China 18, 259–300.

Yuan, D., 1992. The correlation karst development in southwestern and northern China. Quat. Sci. 4, 56–67 (in Chinese).

Zans, V.A., 1959. Recent views on the origin of bauxite. Geonotes 1, 123–132.

Zhang, D., 1982. Analyze the phenomenon of "soil rain" in historical periods. Ke Xue Tong Bao 27, 294–297 (in Chinese).

Zhao, Q.G., 1988. Volcanic ash soils distribution in China. Acta Pedol. Sin. 25, 323–329 (in Chinese).

Zhao, Q.G, Shi, H., 1983. The occurrences, classifies and characteristics of soils in the tropical and subtropical zone districts, China. In: Yen, Q. (Ed.), Chinese Red Soils. Science in China Press, Beijing, pp. 1–23. In Chinese.

Zhou, F., Chen, S.Y., 1994. Geochemical characteristics of lateritic weathering crust in Guigang, Guangxi. J. Cent.South Inst. Min. Metall. 25, 151–155 (in Chinese).

Zhu, B.Q., Mao, C.X., 1983. Nd–Sr isotope and trace element study on Tengchong volcanic rocks from the Indo-Eurasian collisional margin. Geochimica 1, 1–14 (in Chinese).

Zhu, X.M., 1993. Red residua and red soils in southern China. Quater. sci. 1, 75–84 (in Chinese).

Zou, C.G., 1965. The geographical distribution patterns of Soils in Yunnan-Guizhou plateau. Acta Pedologica Sinica 13, 253–261 (in Chinese).